Scientific report
Wetenschappelijk rapport
WR 94-02

Ministerie van Verkeer en Waterstaat

Koninklijk Nederlands
Meteorologisch Instituut

Storm activity over the North Sea and the Netherlands in two climate models compared with observations

Jules J. Beersma

De Bilt, 1994

KNMI

Scientific report
Wetenschappelijk rapport
WR 94-02

De Bilt 1994

Postbus 201
3730 AE De Bilt
Wilhelminalaan 10
Telefoon 030-206 911
Telefax 030-210 407

UDC: 551.513.1
551.553.8
551.515.2
551.583
(261.26)
(492)
ISSN: 0169-1651
ISBN: 90-369-2050-7

Storm activity over the North Sea and the Netherlands in two climate models compared with observations

Jules J. Beersma

Royal Netherlands Meteorological Institute (KNMI),
P.O. Box 201, 3730 AE De Bilt, the Netherlands

E-mail: beersma@knmi.nl

February 1994

Abstract

An intercomparison of wind characteristics over the North Sea and the Netherlands is made between the observations, the control runs of the Canadian Climate Centre (CCC) second generation GCM and the ECHAM coupled ocean-atmosphere GCM, and the enhanced CO_2 runs of these models. Wind direction, wind speed, the frequency of gales (clusters of high wind speeds), the storm track (the time filtered variability of the 500 hPa height) and Empirical Orthogonal Functions (EOFs) of the 500 hPa circulation are considered. In general the differences between the control run and the observations are large. The ECHAM model very poorly reproduces the wind direction distribution and the CCC model strongly underestimates the mean wind speed over sea during summer. The gale frequency is reasonable over land in the ECHAM model but too small over sea in both models. The storm track is in both models less pronounced than in the observations and in the ECHAM model shifted to the south. The average annual amplitudes of the second and third EOFs in the CCC model and those of the three principal EOFs in the ECHAM model differ significantly from the observed ones.

The comparison of the control run and increased CO_2 runs of the models shows only in a few cases a statistical significant change in the wind characteristics. These differences are usually small compared to the differences between the control run and the observations.

Contents

Introduction

On 1 February 1953 an extreme storm coincided with a moderate astronomical spring tide causing severe flooding along the coasts of the Netherlands and eastern England. In response to the deaths of approximately 1800 people the Dutch government appointed the Delta Committee to re-evaluate the height of the sea walls and in the following decades considerable upgrading of the flood defences took place.

There is a general concensus that the anthropogenic increase of greenhouse gases will lead to a global temperature increase (Houghton et al. 1990, 1992). This increase will be largest in the polar regions. Melting of land ice and thermal expansion of the oceans will, with some delay, result in a sea level rise. Up till now it is not clear how the storm activity will respond to this climate forcing. A decrease of the average meridional temperature gradient suggests a decrease of the probability of extreme winds. Warmer oceans, on the other hand, could lead to tropical and mid-latitude cyclones with increased intensities and/or lifetimes. Recently Haarsma et al. (1993) reported that the number of tropical disturbances would increase by 50% under conditions of CO_2 doubling. Their results also indicate that the maximum wind speed of the more intense tropical disturbances increases by about 20%. If this would also be true for extratropical depressions, the flooding probability in the Netherlands with the current sea wall heights will increase. With the 1953 incident in mind the Dutch Ministry of Transport, Public Works and Water Management is very concerned about the future flooding risk.

In this paper the simulated surface wind over the North Sea and the Netherlands in the Canadian Climate Centre (CCC) second generation General Circulation Model (GCM) and the ECHAM coupled ocean-atmosphere GCM in the present climate is compared with observations. For a much larger area, covering most of Western Europe, the simulated 500 hPa circulation in both models is compared with the observed circulation. The 500 hPa circulation determines in which direction weather systems near the surface and thus also storms propagate. The maxima in the geographical distribution of the temporal variability of the 500 hPa height are regarded as 'storm tracks'. An answer is given to the burning question if according to these climate models there are solid indications of a change in the storm activity as a result of increasing greenhouse gas concentrations.

The paper is arranged as follows. Both models and the observations used for comparison are described in section 1. To give an impression of the general performance of the models with respect to the surface wind the average wind direction and the average wind speed are discussed in sections 2 and 3 respectively. The frequency of high wind speeds is taken as an indicator of the storm activity and is discussed in section 4. In section 5 the simulated temporal variability of the geopotential height is compared with observations. In section 6 an objective classification system based on Empirical Orthogonal Eigenfunctions (EOFs) is introduced to study differences in the 500 hPa circulation. In the final section a discussion and conclusions are given.

1 Models and observations

1.1 The CCC second generation GCM

The Canadian Climate Centre second generation general circulation model is described in detail by McFarlane et al. (1992) and Boer et al. (1992). The CCC model consists of a three-dimensional atmospheric general circulation model coupled to a highly simplified ocean. The version considered here has 10 vertical levels and employs a triangular spectral truncation having 32 longitudinal waves (T32/L10). The three-dimensional grid has a horizontal resolution of $3.71° \times 3.75°$. The current climate with a CO_2 concentration of 330 ppm ($1xCO_2$ run) is simulated for a period of 10 years. A second 10 year simulation ($2xCO_2$ run) is obtained with twice the amount of atmospheric CO_2 (660 ppm). The behaviour of the system as it evolves from one to the other of these equilibrium states is not considered. From the European window of the model (224 grid points) four grid points are discussed in detail: two sea points, one north-west and one north-east of the Netherlands hereafter referred to as WS and ES respectively and two land points, one south-west and one south-east of the Netherlands respectively WL and EL. In a map of the area, Figure 1, the locations of the CCC grid points are indicated with a plus (+). For the analysis of the 500 hPa circulation 154 grid points are used. The model output data are archived twice daily at 0000 and 1200 UTC. The 10m wind speed and the 10m u and v-components obtained from the model are averaged over the preceding 12 hours. The 500 hPa heights, however, are 12-hour samples.

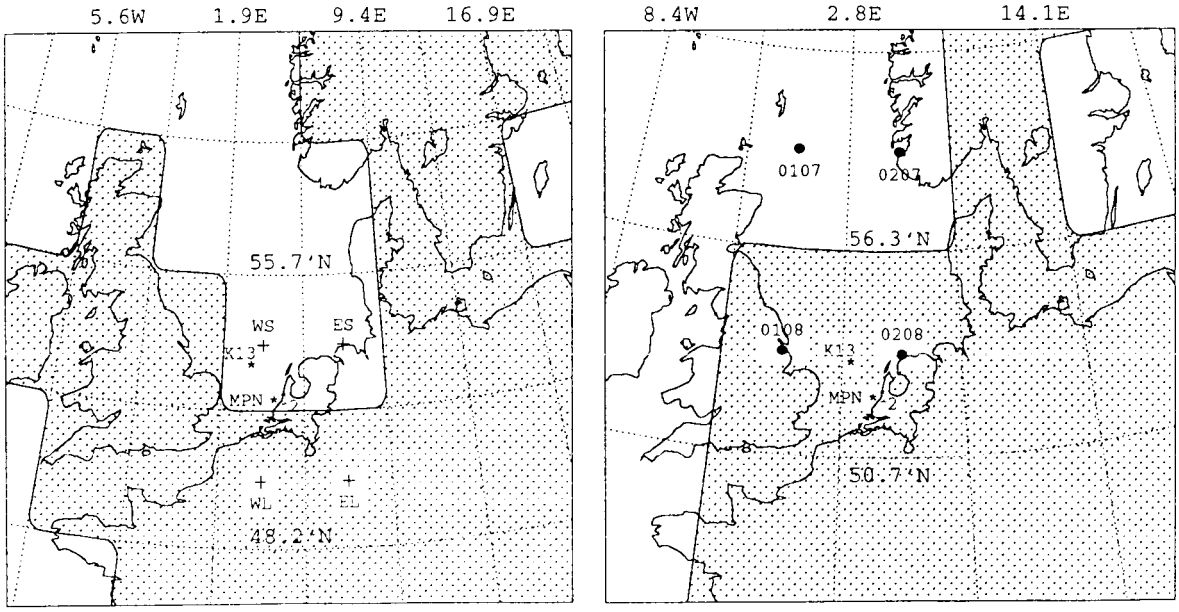

Figure 1: Locations of the grid points over the North Sea and the Netherlands for the CCC model (left) and the ECHAM model (right) relative to the North Sea platforms ($\star$), Schiphol (1) and De Bilt (2). Land grid boxes are shaded.

1.2 The ECHAM coupled ocean-atmosphere model

The atmosphere component (ECHAM) consists of a low resolution version of the spectral numerical weather forecasting model of the European Centre for Medium Range Weather Forecasts (ECMWF) which has been modified extensively at the Max-Planck-Institut für Meteorologie in Hamburg for climate applications. The horizontal resolution of this version (ECHAM1) is limited by 21 triangular spectral waves at 19 vertical levels (T21/L19). The spectral representation is transformed to a $5.6° \times 5.6°$ horizontal grid. The atmosphere model is coupled to the LSG (Large Scale Geostrophic) ocean model. To avoid a climate drift of the coupled system a flux correction is applied. An overview of the model including references to detailed descriptions of various model components is given by Cubasch et al. (1992).

Besides the control run with constant 1985 equivalent CO_2 concentration (390 ppm) which was carried out as a reference the transient $2xCO_2$ run and the IPCC Scenario-A run are considered. The $2xCO_2$ run describes the time-dependent response of the coupled system to a sudden doubling of the atmospheric CO_2 concentration. In this run, the equivalent CO_2 concentration is put at a value of 720 ppm representing a doubling of the CO_2 concentration relative to the level of the early 1970s, rather than 1985. The equivalent CO_2 concentration in the Scenario-A run is based on the 'Business as Usual' greenhouse gas emission scenario (Scenario-A) from the IPCC–report (Houghton et al. 1990) which leads to an equivalent CO_2 doubling-time of 60 years. All simulations were carried out over a 100 year period, from 1985 to 2084. In this paper only the last 10 years (2075–2084) of the three runs are considered. For the Scenario-A run the average CO_2 concentration in this decade is about 2.8 times higher than in 1985 and about 3 times higher than in the early 1970s.

Again four grid points are discussed in detail: one sea point north-west (hereafter referred to as 0106) and one sea point north (0206) of the Netherlands, and two land points; one west of the Netherlands (0107) and one on the Dutch north coast (0207). The locations of the ECHAM grid points are represented in Figure 1 with dots (•). The area selected to study the 500 hPa circulation consists of 80 grid points. The model output is archived twice daily. The modelled 10m u and v-velocity are averaged over the 12 hour output interval and the 500 hPa heights are 12-hour samples. The 10m wind speed itself was not available. Instead a 10m wind speed was calculated as the root of the sum of the squares of the 12-hour averaged 10m u and v-velocities. The resulting average 10m wind speed is then somewhat smaller than the true average 10m wind speed. In real time series the root of the sum of the squares of the 12-hour averaged u and v components is on average about 0.1 m/s smaller than the 12-hour averaged wind speed.

1.3 Observations

The land points are compared with De Bilt (1961–1990; availability: wind speed 100%, wind direction 96%) and Schiphol airport (1981–1991; availability: wind speed 100%, wind direction 95%). The wind at De Bilt and Schiphol is measured at 10 m. For De Bilt the wind measurements are corrected for imperfect station exposure, using gustiness-derived roughness values for each azimuth sector (Wieringa, 1986). The sea

points are compared with platform K13 (1982-1990; availability: wind speed 97%, wind direction 96%) and Measuring Post Noordwijk (hereafter referred to as MPN; 1983-1991; availability: wind speed 93%, wind direction 91%). The locations of the synoptic stations are indicated in Figure 1 with asterisks. The height of the wind measurements at K13 and MPN has changed during the available periods. At K13 the measurement height was 86, 74.9 or 73.8 m above MSL (Mean Sea Level) and at MPN the wind speed and wind direction were measured at 27 or 27.6 m above MSL. The measured wind speeds at K13 and MPN are transformed to 10 m using the logarithmic wind profile. Strictly this transformation holds only for neutral stability. From simultaneous air and seawater temperature measurements at MPN (availability: 78%) stability conditions were calculated (van Wijk et al., 1990) showing that the error in the average monthly wind speed is no more than 6% when stability effects are ignored. The observed time series consist of hourly values which are averaged over 12 hours (0100-1200 and 1300-2400) to make them comparable with the model time series.

ECMWF analyses of the 500 hPa height at 0000 and 1200 UTC for the period 1983-1992 are used to appraise the 500 hPa circulation simulated in the CCC and ECHAM models.

2 The distribution of wind directions

For the frequency distribution of wind directions two periods are distinguished: the period October–March and the period April–September, also referred to as the storm season and the calm season respectively. First the observed distributions of wind direction are discussed and then the simulated wind direction distributions in both models.

2.1 The observed wind direction distributions

The wind direction distributions of Schiphol and De Bilt are presented in Figure 2 for both seasons. As expected these distributions are very similar for the two stations. In both seasons the largest frequencies occur at the south-western directions. A weak secondary maximum is apparent for the north (calm season) and north-eastern (storm season) directions. The frequency distributions of K13 and MPN are shown in Figure 3. These distributions show a close resemblance with those of Schiphol and De Bilt.

2.2 The wind direction distributions in the CCC model

Figure 4 presents the frequency distributions of the $1xCO_2$ and $2xCO_2$ runs for land point WL. Compared with Schiphol and De Bilt the model underestimates the frequency of the north-eastern directions, particularly in the October-March period. This indicates that the model generates too little blocking events. The underestimation of the north-eastern directions is compensated for by an overestimation of the south-western directions. The changes in the wind direction distributions due to the

CO_2 doubling are small compared with the differences between the observations and the control simulation.

The wind direction distributions for sea point WS (Figure 5) are very similar to those for land point WL. The differences of sea point WS with K13 and MPN (Figure 3) are large compared with the differences between K13 and MPN. Again the north-eastern directions are underestimated, and in the storm season the frequencies of the south-western directions are considerably overestimated. The CO_2 doubling also has little effect on the wind direction distributions over the North Sea.

The frequency distributions of the grid points EL and ES are almost identical to those of the grid points WL and WS respectively and are therefore not shown in the figures.

2.3 The wind direction distributions in the ECHAM model

The wind direction distributions of the 1xCO_2, 2xCO_2 and Scenario-A runs for land point 0207 are presented in Figure 6. Compared to the observations, the distributions of the wind directions are very uniform. In the ECHAM control run the direction with the highest frequency is in the storm season south and in the calm season north whereas the observed frequency maximum (Figure 2) is centred around south-west. The changes in the distributions due to a CO_2 increase are small; only the Scenario-A distribution in the storm season shows a perceptible difference.

Figure 7 shows the wind direction distribution of the three runs for sea point 0206. Again the distributions are rather uniform. The most frequent directions in the control run are east and north for the storm season and the calm season respectively. The observed peak centered round south-west (Figure 3) is lacking again. As before the changes in the distributions due to increased CO_2 concentrations are small, also in the storm season for the Scenario-A distribution.

The distibutions of the grid points 0107 and 0106 are very similar to those of 0207 and 0206 respectively and therefore not included as figures.

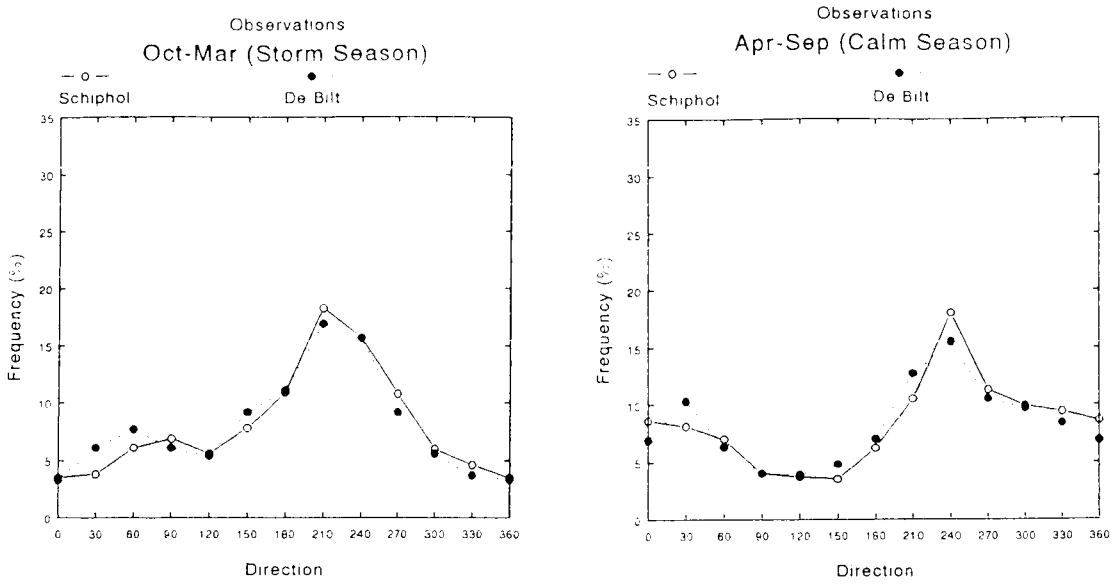

Figure 2: Observed wind direction frequencies (%) over *land* in the storm season (left panel) and in the calm season (right panel)

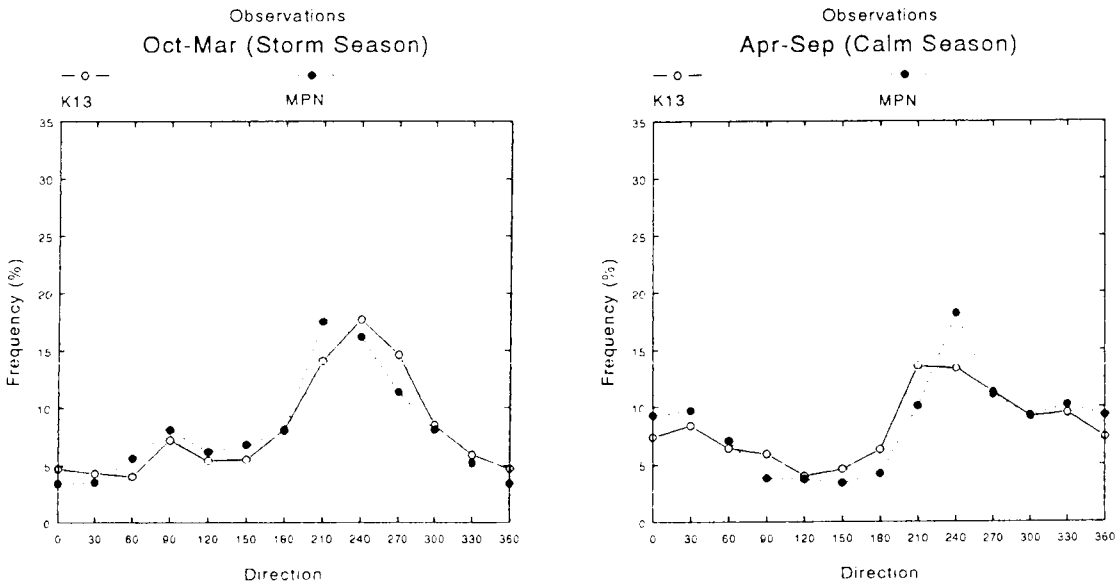

Figure 3: Observed wind direction frequencies (%) over *sea* in the storm season (left panel) and in the calm season (right panel)

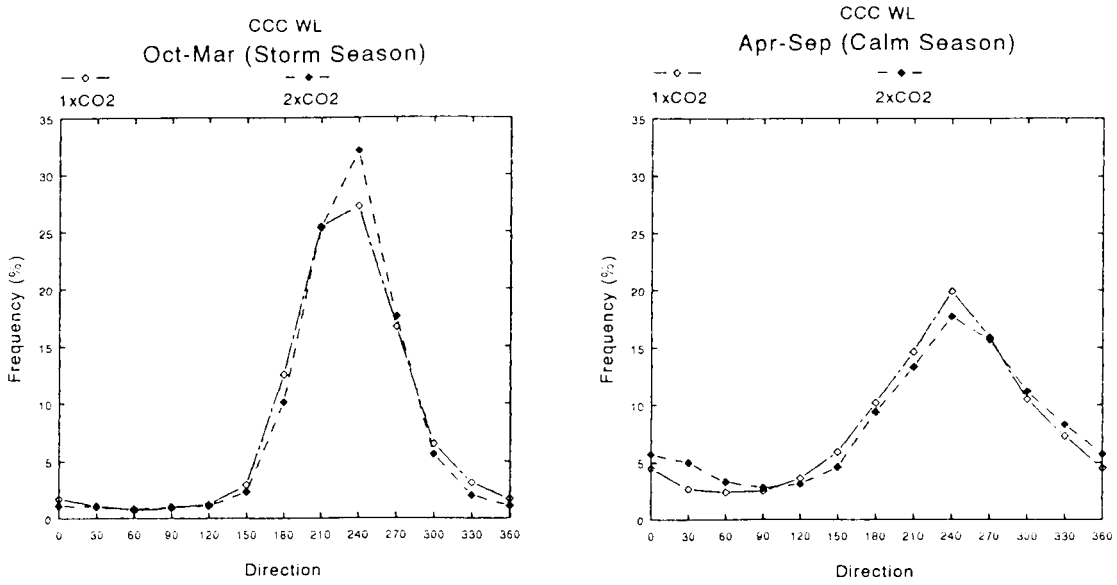

Figure 4: Wind direction frequencies (%) for CCC *land* point WL in the storm season (left panel) and in the calm season (right panel)

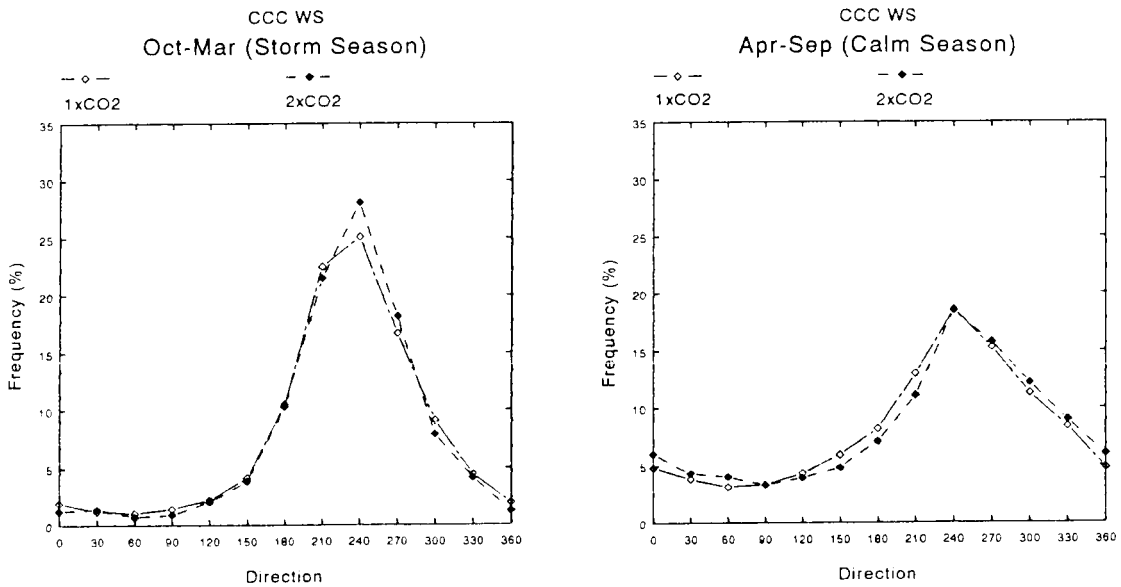

Figure 5: Wind direction frequencies (%) for CCC *sea* point WS in the storm season (left panel) and in the calm season (right panel)

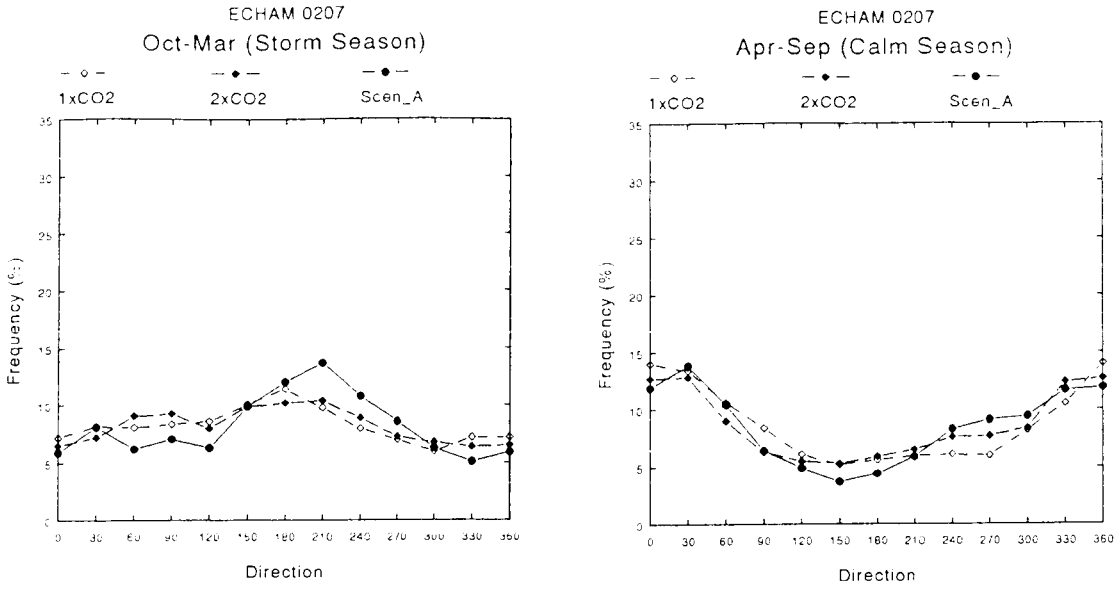

Figure 6: Wind direction frequencies (%) for ECHAM *land* point 0207 in the storm season (left panel) and in the calm season (right panel)

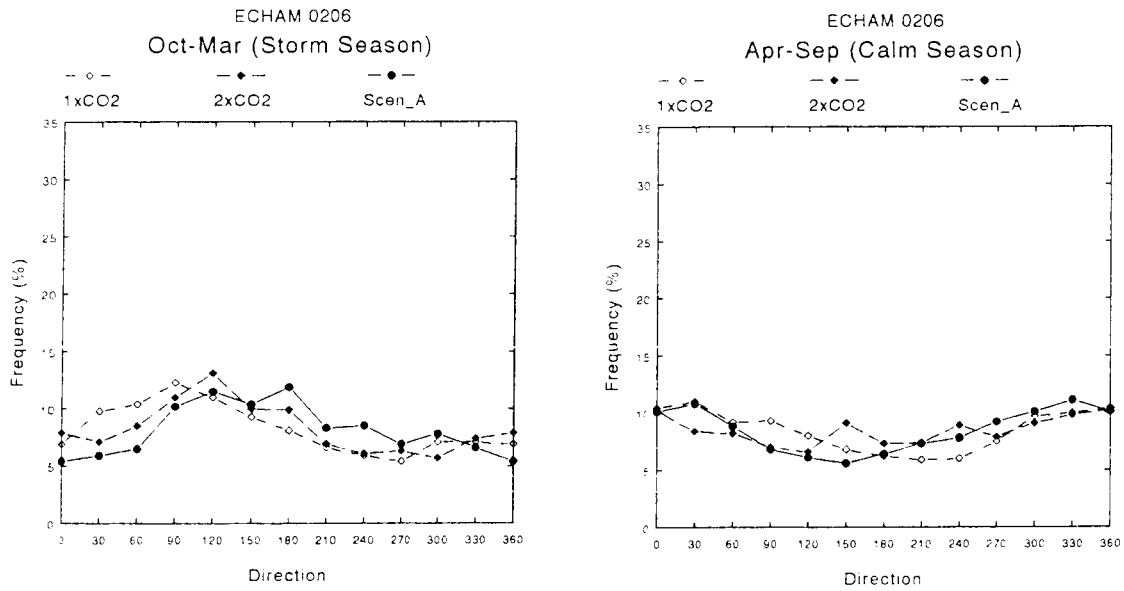

Figure 7: Wind direction frequencies (%) for ECHAM *sea* point 0206 in the storm season (left panel) and in the calm season (right panel)

3 Average wind speed

3.1 Observed average wind speeds

Figure 8 shows the annual cycle of the average wind speeds at Schiphol, De Bilt, K13 and MPN. The average wind speed at Schiphol, which is closer to the sea, is about 2 m/s higher in winter and about 1 m/s higher in summer than at De Bilt. As a consequence, the amplitude of the annual cycle at Schiphol is somewhat larger than at De Bilt.

The average wind speeds at K13 are about 1 m/s higher than at MPN except for the period June–September where they are almost equal. As expected, the average wind speeds over sea are several metres per second higher than over land. The annual cycle is also larger over sea.

3.2 Average wind speeds in the CCC model

The annual cycles of the average wind speeds in the control run and the perturbed run for land point WL and sea point WS are shown in Figure 9. The average wind speeds for land point WL in the control run well reproduce the observed averages at De Bilt. Contrarily, the annual cycle of the average wind speed for sea point WS differs markedly from the baseline stations K13 and MPN. In summer the speed is up to 4 m/s too small compared to MPN as well as K13 while in the October–February period it is not much different from the observations. Very remarkable is that for sea point WS the average wind speed in summer is even *smaller* than that for the adjacent land point WL. This paradoxical effect is also manifest at neighbouring sea points and may be related to stability effects.

For both grid points the changes in average monthly wind speed due to the CO_2 doubling are typically within 1 m/s. In the storm season the seasonally averaged wind speed for both grid points increases by about 0.2 m/s. In the calm season the seasonally averaged wind speed decreases for the grid points WL and WS with about 0.3 m/s.

The average wind speeds for land point EL and sea point ES, which are not presented in the figures, are somewhat smaller than those for land point WL and sea point WS respectively. The amplitude of the annual cycle is virtually the same. The difference in seasonally averaged wind speed between the $2xCO_2$ and the $1xCO_2$ climate is for the grid points EL and ES about 0.1 m/s smaller than for the grid points WL and WS.

3.3 Average wind speeds in the ECHAM model

The average monthly wind speeds in the control run for land point 0207, shown in Figure 10a, lie between those at Schiphol and those at De Bilt (Figure 8a). For sea point 0206, the average wind speeds presented in Figure 10b are for all months about 2 m/s smaller than those at K13 and MPN. There is, however, a rather large separation between this sea point and the platforms K13 and MPN (Figure 2). From

a study of observations from ships and lightvessels by Korevaar (1990) it is expected that the sea points 0106 and 0206 should have a larger average wind speed than the platforms K13 and MPN. (See section 4.2 for further details.) The differences between the average wind speed over sea in the ECHAM model and the observed wind are thus even larger than suggested by Figure 10b. The amplitude of the annual is realistic however.

The changes due to a CO_2 increase are for both grid points very small. Grid points 0107 and 0106, which are not presented in the figures, have somewhat higher average wind speeds than grid points 0207 and 0206 respectively. Apart from a 0.6 m/s larger decrease of grid point 0106 compared with grid point 0206 in the Scenario-A run for the storm season, the changes in the average wind speed due to CO_2 increases are for the grid points 0106 and 0107 of the same size as those for the grid points 0206 and 0207.

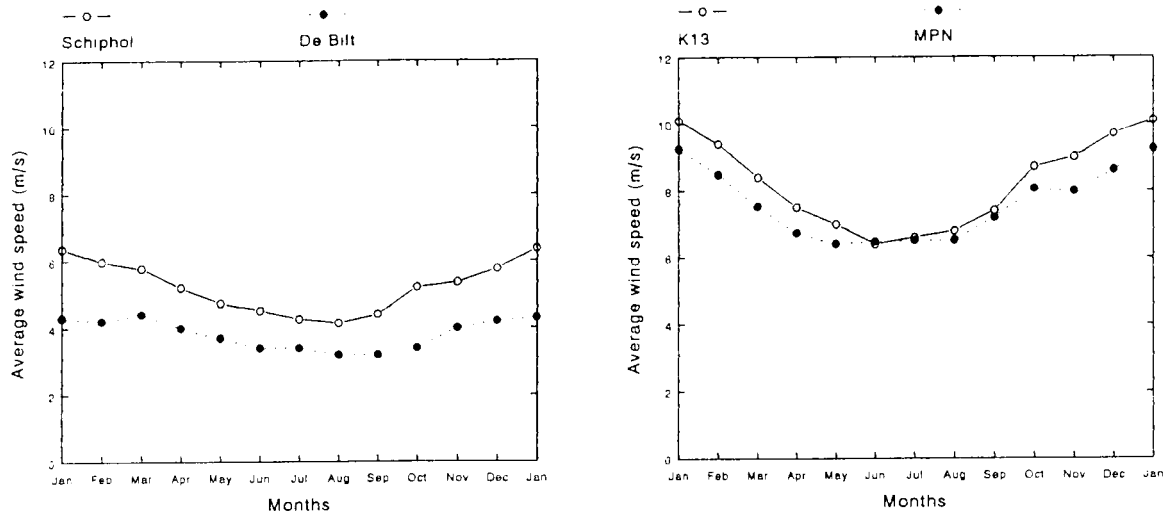

Figure 8: Observed average monthly wind speeds over *land* (left panel) and over *sea* (right panel)

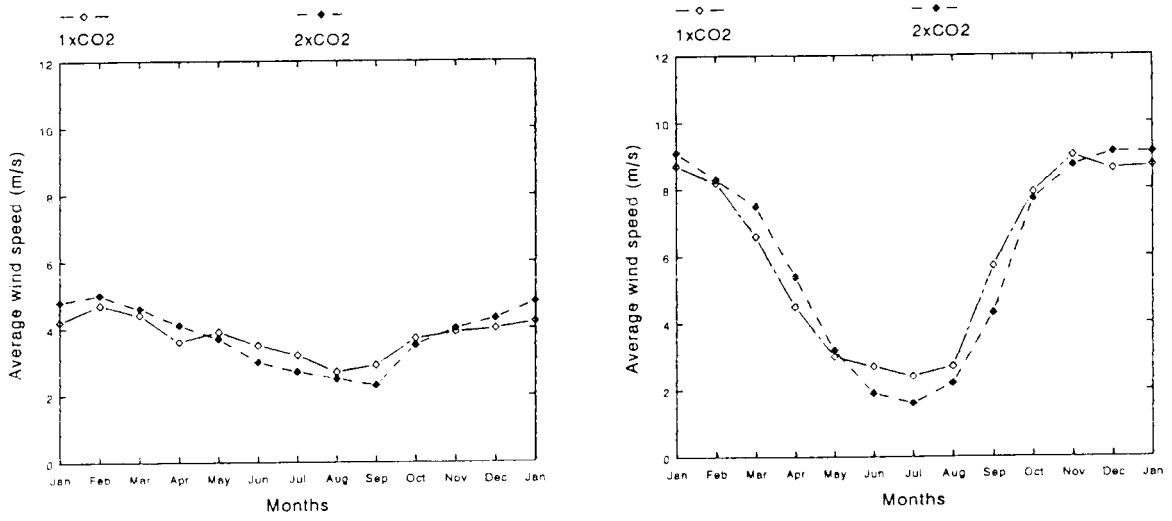

Figure 9: Average monthly wind speeds for CCC *land* point WL (left panel) and *sea* point WS (right panel)

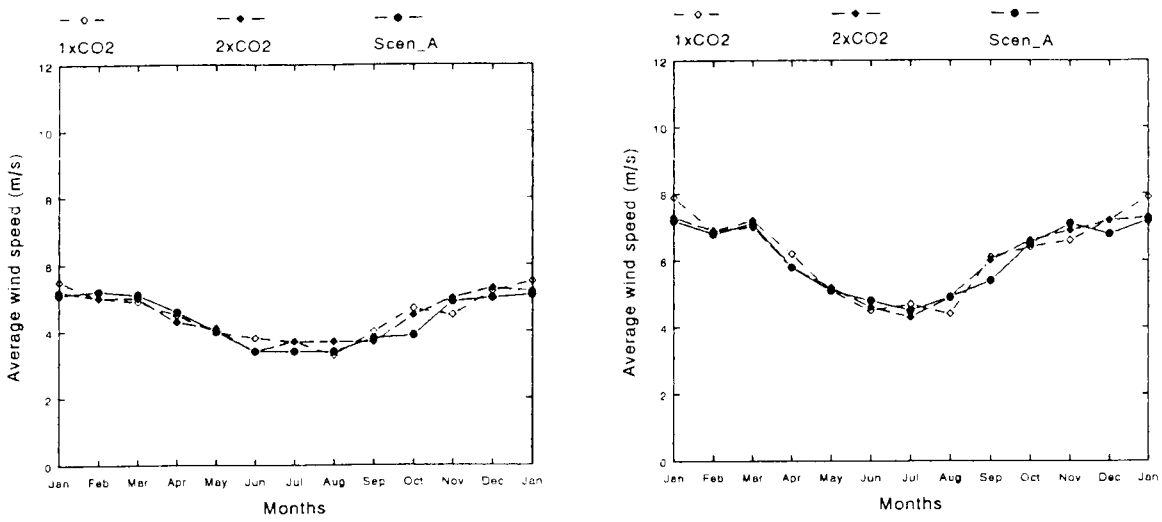

Figure 10: Average monthly wind speeds for ECHAM *land* point 0207 (left panel) and *sea* point 0206 (right panel)

4 The frequency of high wind speeds

High wind speeds usually occur in clusters. A gale consists of a cluster of consecutive high wind speeds. To test for differences in the frequency of high wind speeds it is more convenient to look at the number of clusters of high wind speeds than at the number of individual extremes. Several definitions of clusters are possible. Gales following from two different cluster definitions will be used. The first definition is the 'run' definition. A run is a group of consecutive exceedances of a specified threshold, preceeded and followed by a value below that threshold. The second cluster definition, the 'block' definition, is obtained by dividing the n observations in smaller 'blocks' of specified size and regarding one or more exceedances of the threshold in any one block as forming a cluster. A drawback of the run definition is that it may split two or more nearby but separated groups that should in reality be regarded as just one cluster. On the other hand, the block definition may split a single cluster and combine two or more into one. For 'smoothly varying' observations the run definition seems preferable in avoiding the ambiguity of block size choices. However, in the case of missing data the block definition is superior and in general theoretically more tractable. To determine the frequency of high wind speeds we used 'runs' and 'blocks of size 5 (60 hours)'.

For a sufficiently high threshold the stochastic process generated by the cluster positions is approximatly a Poisson process. Details about this Poisson limit are given in Hsing et al. (1988) and Smith (1988). The test for equality of the rates of two independent Poisson processes in Cox and Hinkley (1974, pp 136–137) was used to test for differences in high wind speed frequencies between the observations and a control run and between two independent model runs. The hypothesis of equal occurrence rates was tested at the 5%-level. The test still applies when there are missing values in the observed record as long as the interruptions in the observed winds are independent of the occurrences of high wind speeds.

What remains to be discussed is the choice of the threshold values. On the one hand, the threshold should be large enough to obtain a Poisson process; on the other hand it should be so low that a sufficient number of threshold exceedances remains. These conflicting requirements prevent a fixed threshold choice. As a consequence, the thresholds for the year and the storm season (October–March) were chosen about 2–3 m/s higher than for the calm season (April–September) and over sea the threshold was taken about 5 m/s higher than over land.

4.1 Gales in the CCC model compared with observations

The number of gales (runs and blocks) per year and season for the land points WL and EL, Schiphol and De Bilt is presented in Table 1. For the land points WL and EL the number of gales is smaller than observed. This holds even for De Bilt despite of its agreement with the average wind speed of WL (Figures 8a and 9a). Because an approximately 2 m/s higher average wind speed was found at Schiphol than at De Bilt it is not surprising that also the number of gales is higher at Schiphol. Apart from the case WL, De Bilt in the calm season, the differences are significant at the 5%-level.

Table 2 shows the changed number of clusters for the land points WL and EL due to the CO_2 doubling. In the storm season there is a small increase of the number of gales for the grid point WL and a small decrease for the grid point EL, though not significant at the 5%-level. In the calm season the changes are very small.

For the sea points WS and ES, K13 and MPN the number of gales per year and season is shown in Table 3. Again the number of gales in the model is significantly smaller than in the observations. Only one case, the number of runs for the sea point WS compared with MPN in the storm season, is not significant at the 5%-level.

Tabel 4 shows the change in the number of clusters for the sea points WS and ES as a result of the doubling of the CO_2 concentration. In the storm season and over the year there is for both sea points an increase of the number of clusters which is statistically significant for sea point WS only. In the calm season there is a very small decrease for sea point WS and a small increase for sea point ES.

The Dutch coast is mainly endangered by the north-west component of a storm. To evaluate this, the winds were projected onto the north-west direction (315°) and the winds with large positive north-west component were considered. Table 5 gives the number of gales with a large north-west component for the sea points WS and ES, MPN and K13. In all cases the number of gales for the sea points is significantly smaller than observed. In the storm season these differences are even larger than those in Table 3. This is, however, consistent with Figures 3 and 5 which show that the model underestimates the frequency of northern wind directions.

The numbers of gales for K13 and MPN in Table 5 are almost equal while in Table 3 the number of gales for K13 is larger in all cases. This shows that at K13 there are more gales with a small north-west component.

Table 6 shows that the changes in the number of clusters with a large north-west component due to the CO_2 doubling are small.

To evaluate whether the results for individual grid points (not much change in case of CO_2 doubling, Tables 2 and 4) also apply to a larger area, two areas of 8 adjacent grid points are selected; one over the North Sea extending to 63°N and one over land centered at 48.2°N, 5.6°E. The average number of gales and the average of the maximum number of gales in the sea and the land area are calculated. The first average is obtained by averaging the number of gales over the various grid points in the area and over the years or seasons. For the average maximum the grid point with the largest number of gales in each year or season is considered. The results for the control and perturbed simulation are given in Table 7. The average numbers of gales for the sea area and for the land area are comparable with those for sea point WS (Table 4) and those for land point EL (Table 2) respectively. The differences between the average number of gales and the average of the maximum number of gales are larger for the land area than for the sea area. This indicates that the number of gales is less uniformly distributed over the land area than over the sea area. A more detailed analysis reveals a considerable decrease in the number of gales eastwards over the land area. This is obviously related with the roughness transition at the west coast of Europe and the decrease in the activity of depressions as soon as they reach the continent.

The average number of gales and the average of the maximum number of gales

are not Poisson distributed and therefore the statistical significance of the differences between the $2xCO_2$ and the control run is not tested as before but using Student's t-statistic. In this set the significance level of 5% was never reached.

4.2 Gales in the ECHAM model compared with observations

Table 8 compares the number of gales for the land points 0107 and 0207 with those of Schiphol and De Bilt. The number of gales of land point 0207 is in all cases between those at Schiphol and those at De Bilt. The 0107 values are in all cases closer to those of Schiphol than those of De Bilt. Although the average wind speed over land in the ECHAM model is only a little higher than that in the CCC model (Figures 9 and 10), the ECHAM model, with its lower resolution, generates much more clusters with high wind speeds than the CCC model (Table 1).

Table 9 shows for the land points 0107 and 0207 the number of gales in the control, $2xCO_2$ and Scenario-A simulations. In the storm season the perturbed simulations have for both land points a larger number of gales than the control simulation, but this difference is only in one case statistically significant. In the calm season there are increases as well as decreases of the number of gales but none of the differences is significant at the 5%-level.

Table 10 compares the numbers of gales of the sea points 0106 and 0206 with those of MPN and K13. For both sea points the number of gales is smaller than in the observations. In many cases, this difference is statistically significant. It should be noted, however, that the locations of the sea points 0106 and 0206 are relatively far from the locations of the platforms K13 and MPN. Korevaar (1990) gives wind speed exceedance frequencies based on observations from ships and lightvessels. From these exceedance frequencies it follows that in the storm season the value 7 Bft ($\approx$ 13.9 m/s) is about twice more often exceeded at the positions of the sea points 0106 and 0206 than at the positions of the platforms K13 and MPN. Therefore the differences between the number of gales over sea in the ECHAM model and the observations are in fact larger than suggested in Table 10. Hulme et al. (1993) found an underestimation of about 50 % of the number of gales over the seas around the British Isles (50°–60°N; 10°W–2°E) for the same ECHAM model as well as for a high-resolution version of the UK Meteorological Office atmospheric model.

The change of the number of gales of the ECHAM sea points 0106 and 0206 due to CO_2 increases is presented in Table 11. These changes are not significant at the 5% level. If any effect occurs, the number of gales decreases for sea point 0106 due to a CO_2 doubling in the storm season but increases in all other cases of that season, while in the calm season the number of clusters is decreasing in all cases.

Table 12 represents the ECHAM analogon of Table 7. The two areas under consideration are at about the same positions as before (section 4.1), but consist now of 6 adjacent grid points each. The average number of gales for the sea area and for the land area are comparable with those for sea point 0106 (Table 11) and those for land point 0207 (Table 9) respectively. The differences between the average number of gales and the average of the maximum number of gales are somewhat larger for

the land area than for the sea area. Both the land area and the sea area show an eastward decrease of the number of gales but not as rapid as in the CCC model over the land area. This could be related with the model-generated 500 hPa trough over Central Europe (see section 6.3 and Figure 17, upper left pannel).

The increase of the average number of runs for the land area in the storm season due to the CO_2 doubling is significant at the 5%-level as for land point 0207, in Table 9, under the same conditions. In the calm season the decrease of the number of gales for the land area due to the CO_2 doubling is just significant at the 5%-level. It should be noted, however, that when 48 tests at the 5%-level are performed as in Table 12 one would expect 2 or 3 rejections of the null hypothesis if the null hypothesis were true in all cases. So there is in fact no statistical evidence of a systematic change in the average number of gales in the perturbed simulations.

Table 1: Average number of gales with a wind speed threshold of d m/s for observations and the CCC *land* points WL and EL.

	d	Schiphol	De Bilt	WL	EL
year					
runs	12	8.7	1.1	0.3 ^{sb}	0 ^{sb}
blocks	12	9.0	1.1	0.3 ^{sb}	0 ^{sb}
Oct – Mar					
runs	12	8.2	1.0	0.3 ^{sb}	0 ^{sb}
blocks	12	8.5	1.0	0.3 ^{sb}	0 ^{sb}
Apr – Sep					
runs	9	6.1	1.1	0.6 ^{s}	0.3 ^{sb}
blocks	9	6.6	1.2	0.6 ^{s}	0.3 ^{sb}

$^{s(b)}$ differences with respect to Schiphol (De Bilt) significant at the 5%–level

Table 2: Average number of gales with a wind speed threshold of d m/s for the CCC *land* points WL and EL in the control and the perturbed simulations.

		WL		EL	
	d	$1xCO_2$	$2xCO_2$	$1xCO_2$	$2xCO_2$
year					
runs	9	7.4	9.1	2.7	1.7
blocks	9	7.3	8.5	2.8	1.8
Oct – Mar					
runs	9	6.8	8.7	2.4	1.7
blocks	9	6.7	8.1	2.5	1.8
Apr – Sep					
runs	7	5.7	5.8	2.4	2.5
blocks	7	5.7	5.7	2.5	2.7

no significant differences between $2xCO_2$ and $1xCO_2$ at the 5% level

Table 3: Average number of gales with a wind speed threshold of d m/s for observations and the CCC *sea* points WS and ES.

	d	MPN	K13	WS	ES
year					
runs	17	4.0	7.1	2.2 ^{mk}	1.6 ^{mk}
blocks	17	4.4	7.3	2.2 ^{mk}	1.5 ^{mk}
Oct – Mar					
runs	17	3.7	6.4	2.1 ^{k}	1.6 ^{mk}
blocks	17	3.9	6.5	2.1 ^{mk}	1.5 ^{mk}
Apr – Sep					
runs	14	3.4	4.6	1.2 ^{mk}	0.5 ^{mk}
blocks	14	3.9	4.6	1.2 ^{mk}	0.5 ^{mk}

$^{m(k)}$ differences with respect to MPN (K13) significant at the 5%–level

Table 4: Average number of gales with a wind speed threshold of d m/s for CCC *sea* points WS and ES in the control and perturbed simulations.

		WS		ES	
	d	1xCO_2	2xCO_2	1xCO_2	2xCO_2
year					
runs	17	2.2	3.9*	1.6	2.6
blocks	17	2.2	3.9*	1.5	2.4
Oct – Mar					
runs	17	2.1	3.8*	1.6	2.6
blocks	17	2.1	3.8*	1.5	2.4
Apr – Sep					
runs	12	3.6	3.5	2.5	2.8
blocks	12	3.7	3.6	2.9	3.0

* differences between 2xCO_2 and 1xCO_2 significant at the 5% level

Table 5: Average number of gales with a north-west component larger than d m/s for observations and the CCC *sea* points WS and ES.

	d	MPN	K13	WS	ES
year					
runs	14	3.2	3.6	0.5 ^{mk}	0.3 ^{mk}
blocks	14	3.4	3.7	0.6 ^{mk}	0.3 ^{mk}
Oct – Mar					
runs	14	2.9	2.9	0.5 ^{mk}	0.2 ^{mk}
blocks	14	3.0	2.8	0.6 ^{mk}	0.2 ^{mk}
Apr – Sep					
runs	11	3.6	3.7	0.5 ^{mk}	0.5 ^{mk}
blocks	11	4.7	4.8	0.5 ^{mk}	0.5 ^{mk}

$^{m(k)}$ differences with respect to MPN (K13) significant at the 5%-level

Table 6: Average number of gales with a north-west component larger than d m/s for the CCC *sea* points WS and ES in the control and perturbed simulations.

		WS		ES	
	d	$1xCO_2$	$2xCO_2$	$1xCO_2$	$2xCO_2$
year					
runs	11	5.5	5.2	3.8	3.9
blocks	11	5.6	5.2	4.1	3.8
Oct – Mar					
runs	11	5.0	4.5	3.3	3.0
blocks	11	5.1	4.4	3.5	2.9
Apr – Sep					
runs	9	2.7	2.9	2.3	2.5
blocks	9	2.8	3.2	2.5	2.9

no significant differences between $2xCO_2$ and $1xCO_2$ at the 5%-level

Table 7: Average number of gales in a sea area and a land area with a wind speed threshold of d m/s in the CCC control and perturbed simulations. The average (av) is obtained by averaging the number of gales over the various grid points and over the years or seasons; for the average of the maximum (max) the grid point with the largest number of gales in each year or season is considered.

		runs		blocks	
	d	$1xCO_2$	$2xCO_2$	$1xCO_2$	$2xCO_2$
year					
Sea area(av)	17	2.1	2.5	2.2	2.6
Sea area(max)	17	4.2	4.8	4.6	5.0
Land area(av)	9	2.9	3.0	2.8	3.0
Land area(max)	9	10.7	12.1	10.4	12.0
Oct – Mar					
Sea area(av)	17	1.9	2.5	2.0	2.5
Sea area(max)	17	3.9	4.5	4.0	4.6
Land area(av)	9	2.6	2.9	2.7	2.9
Land area(max)	9	9.8	11.3	10.1	11.2
Apr – Sep					
Sea area(av)	12	3.9	3.7	4.4	4.0
Sea area(max)	12	6.4	5.8	6.8	6.4
Land area(av)	7	2.3	2.4	2.3	2.5
Land area(max)	7	7.1	8.1	7.7	8.8

no significant differences between $2xCO_2$ and $1xCO_2$ at the 5% level

Table 8: Average number of gales with a wind speed threshold of d m/s for observations and the ECHAM *land* points 0107 and 0207.

	d	Schiphol	De Bilt	0107	0207
year					
runs	12	8.7	1.1	6.8 ^{b}	2.6 ^{sb}
blocks	12	9.0	1.1	8.3 ^{b}	3.0 ^{sb}
Oct – Mar					
runs	12	8.2	1.0	5.5 ^{sb}	2.1 ^{s}
blocks	12	8.5	1.0	6.9 ^{b}	2.5 ^{sb}
Apr – Sep					
runs	9	6.1	1.1	6.2 ^{b}	3.5 ^{sb}
blocks	9	6.6	1.2	7.4 ^{b}	4.0 ^{sb}

$^{s(b)}$ differences with respect to Schiphol (De Bilt) significant at the 5% level

Table 9: Average number of gales with a wind speed threshold of d m/s for the ECHAM *land* points 0107 and 0207 in the control and the perturbed simulations.

	d	0107			0207		
		$1xCO_2$	$2xCO_2$	Scen_A	$1xCO_2$	$2xCO_2$	Scen_A
year							
runs	12	6.8	7.4	7.8	2.6	4.0	2.4
blocks	12	8.3	8.3	9.4	3.0	4.0	2.7
Oct – Mar							
runs	12	5.5	6.6	6.8	2.1	3.9*	2.3
blocks	12	6.9	7.5	8.2	2.5	3.9	2.6
Apr – Sep							
runs	9	6.2	6.4	6.8	3.5	2.3	2.6
blocks	9	7.4	7.2	8.3	4.0	2.5	3.1

* difference with respect to $1xCO_2$ significant at the 5%-level

Table 10: Average number of gales with a wind speed threshold of d m/s for observations and the ECHAM *sea* points 0106 and 0206.

	d	MPN	K13	0106	0206
year					
runs	17	4.0	7.1	2.5^{k}	1.0^{mk}
blocks	17	4.4	7.3	2.5^{k}	1.1^{mk}
Oct – Mar					
runs	17	3.7	6.4	2.4^{k}	0.9^{mk}
blocks	17	3.9	6.5	2.4^{k}	1.0^{mk}
Apr – Sep					
runs	14	3.4	4.6	1.9^{k}	1.0^{mk}
blocks	14	3.9	4.6	2.1^{mk}	1.0^{mk}

$^{m(k)}$ differences with respect to MPN (K13) significant at the 5%-level

Table 11: Average number of gales with a wind speed threshold of d m/s for the ECHAM *sea* points 0106 and 0206 in the control and the perturbed simulations.

	d	0106			0206		
		$1xCO_2$	$2xCO_2$	Scen_A	$1xCO_2$	$2xCO_2$	Scen_A
year							
runs	17	2.5	2.5	3.2	1.0	1.5	1.9
blocks	17	2.5	2.5	3.5	1.1	1.7	2.1
Oct – Mar							
runs	17	2.4	2.1	3.0	0.9	1.2	1.9
blocks	17	2.4	2.1	3.2	1.0	1.4	2.1
Apr – Sep							
runs	12	4.6	3.8	3.7	3.5	2.9	2.4
blocks	12	5.2	4.6	4.5	4.3	3.3	2.7

no significant differences with respect to $1xCO_2$ at the 5%–level

Table 12: Average number of gales in a sea area and a land area with a wind speed threshold of d m/s in the ECHAM control and perturbed simulations. The average (av) is obtained by averaging the number of gales over the various grid points and over the years or seasons; for the average of the maximum (max) the grid point with the largest number of gales in each year or season is considered.

	d	runs			blocks		
		$1xCO_2$	$2xCO_2$	Scen_A	$1xCO_2$	$2xCO_2$	Scen_A
year							
Sea area(av)	17	2.5	2.5	2.8	2.9	2.7	3.1
Sea area(max)	17	5.6	5.4	4.7	6.2	5.9	5.5
Land area(av)	12	2.3	2.7	2.0	2.7	3.0	2.4
Land area(max)	12	6.7	7.2	7.8	8.4	8.3	9.4
Oct – Mar							
Sea area(av)	17	2.4	2.3	2.7	2.8	2.5	3.0
Sea area(max)	17	5.1	4.9	4.7	5.6	5.2	5.4
Land area(av)	12	1.8	2.7*	1.9	2.2	3.0	2.3
Land area(max)	12	5.2	6.7	7.2	6.6	7.7	8.8
Apr – Sep							
Sea area(av)	12	4.4	4.1	4.0	5.5	5.4	5.1
Sea area(max)	12	7.4	7.0	6.5	9.0	9.5	8.9
Land area(av)	9	2.3	1.8*	1.9	2.8	2.1*	2.3
Land area(max)	9	6.1	6.2	6.6	7.5	7.2	8.3

* differences with respect to $1xCO_2$ significant at the 5%–level

5 Storm tracks

From the geographical distribution of the temporal variance of the 500 hPa geopotential height the location and intensity of the storm tracks can be determined. Sawyer (1970) found that his low-frequency (20 60 days) field exhibited maxima in regions characterized by frequent blocking activity while his higher frequency field (< 10 days) was closely linked to the major cyclone tracks. Blackmon (1976) suggests that his high-frequency (1–2 days) variability is partially due to the diurnal tide and partially spurious and therefore undesirable. Following Blackmon (1976) and Lau (1988) the maxima in the root-mean-square (rms) of bandpass (2.25–6 days) filtered geopotential height are considered as the 'storm tracks' with the understanding that these storm tracks portray the preferred propagation paths of both cyclones and anti-cyclones as Wallace et al. (1988) have pointed out.

5.1 The storm track over Western Europe

The storm track over Western Europe is the tail end of the North Atlantic storm track which initiates over eastern North America and terminates over the west coast of Europe. For convenience only the storm track for the storm season (Oct–Mar) is considered.

The rms of bandpass filtered 500 hPa height from the 9 complete storm seasons in the 1983–1992 ECMWF analyses is presented in Figure 11. Both the position and the intensity of the storm track correspond very well with the rms of bandpass filtered 500 hPa height for the climatological winter given in Blackmon (1976).

5.2 The storm track in the CCC model

The storm tracks for the 10 complete storm seasons in the CCC control and $2xCO_2$ simulations are shown in Figure 12. In the control run of the CCC model the time filtered variability is much smaller compared with the observations. It turns out to be comparable with the observed time filtered variablity in the calm season (not shown). The CCC model reproduces the position of the storm track quite well. Lambert (1988) extracted cyclone climatology from a 5-year simulation of an earlier version of the CCC model and found in the Northern Hemisphere winter (DJF) a deficiency of weak cyclones and an excess of intense cyclones while the number of cyclones of medium intensity is well simulated. The changes in the time filtered variability pattern due to CO_2 doubling are in general small. The most striking effects are an increase in variability over the northern North Sea and beyond, together with a decrease of variability over south Europe.

5.3 The storm track in the ECHAM model

Figure 13 shows the time filtered variability for the 9 complete storm seasons in the ECHAM control and the perturbed experiments. The time filtered variability is much smaller than in the observations. Roeckner et al. (1992) attribute this to a too weak

circulation over the North Atlantic in the ECHAM model. The band of maximum variability is less pronounced and shifted south compared to the observations. As before, this seems to be the result of the mid-European trough in the 500 hPa flow in the ECHAM model (Figure 17, upper left pannel). The time filtered variability of the $2xCO_2$ and the Scenario-A simulations shows hardly any difference with that of the control simulation.

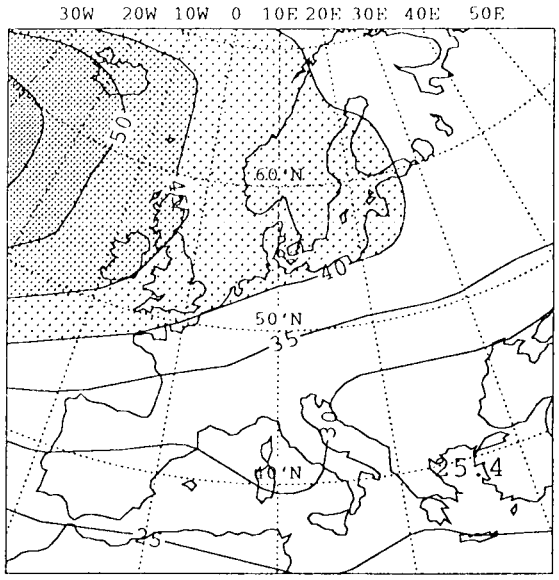

Figure 11: Root-mean-square (rms) of the 1983–1992 bandpass filtered 500 hPa height in the 9 complete storm seasons (Oct–Mar). Contour interval is 5 m. The areas with rms values exceeding 40 m are shaded.

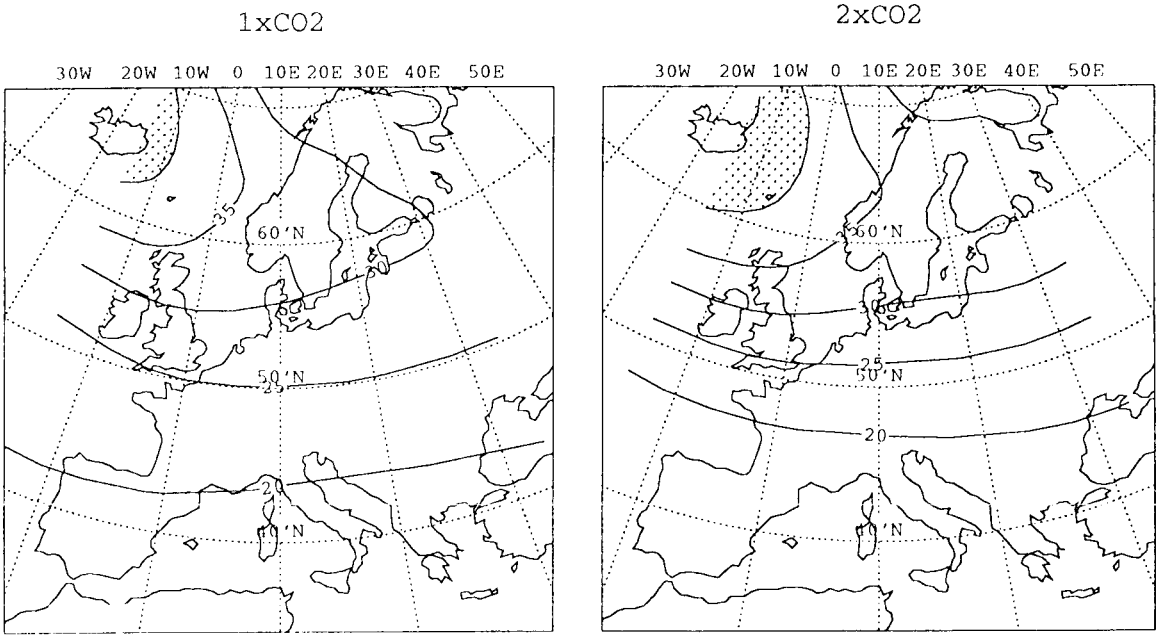

Figure 12: Root-mean-square (rms) of bandpass filtered 500 hPa height in the 10 complete storm seasons (Oct Mar) for the CCC control simulation (left panel) and the $2xCO_2$ simulation (right panel). Contour interval is 5 m. The areas with rms values exceeding 40 m are shaded.

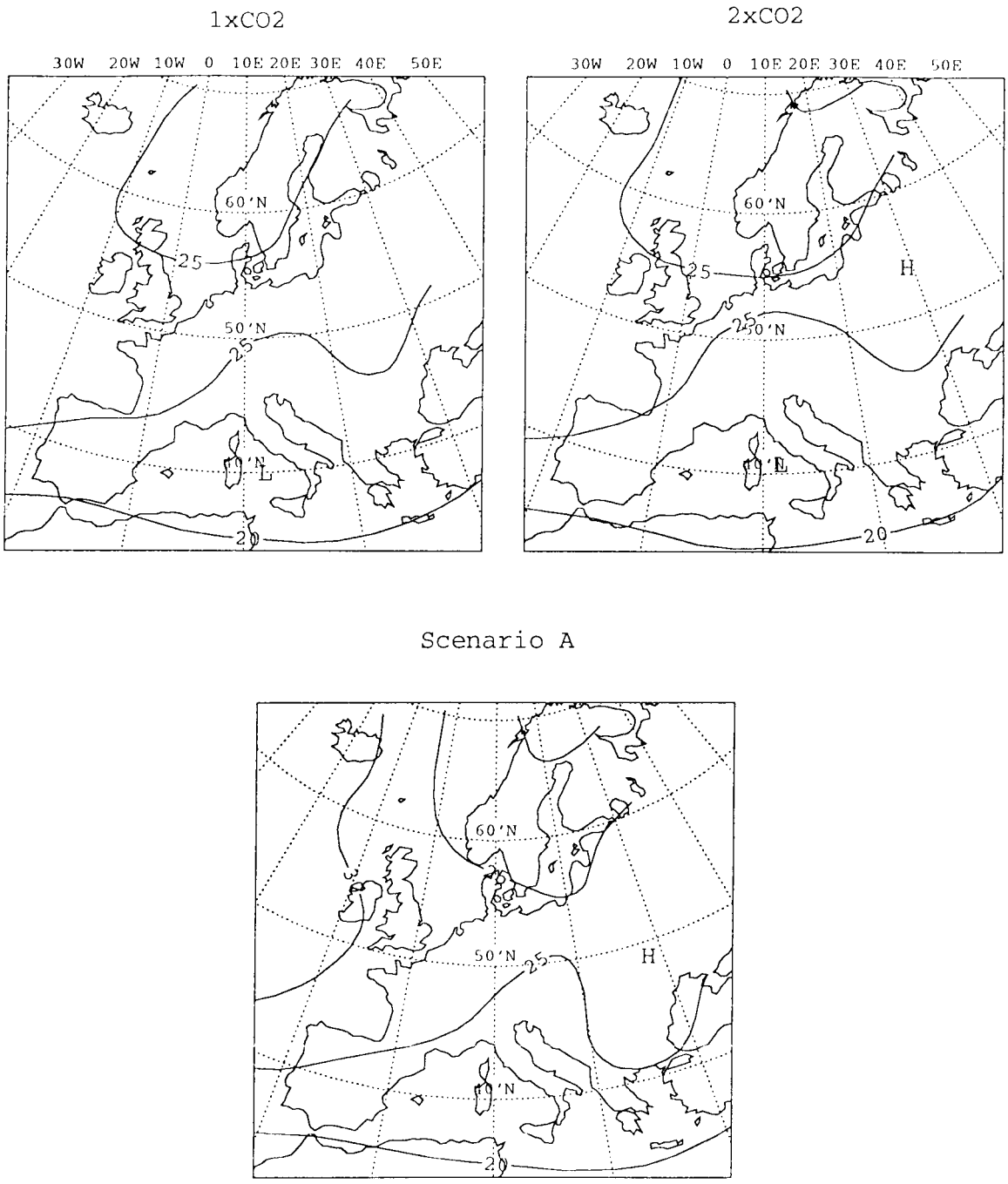

Figure 13: Root-mean-square (rms) of bandpass filtered 500 hPa height in the 9 complete storm seasons (Oct–Mar) for the ECHAM control simulation (upper left panel), the 2xCO_2 simulation (upper right panel) and the Scenario-A simulation (lower panel). Contour interval is 5 m.

6 EOF analysis of the 500 hPa circulation

The major virtue of Empirical Orthogonal Function (EOF) analysis is the reduction of the dimensionality of a large data set. The data is approximated by a small set of variables that retains most of the variation present in all of the original variables. Computation of the EOFs reduces to the solution of an eigenvalue-eigenvector problem. The scalar variable $\phi(x,t)$, at N positions x and T distinct times t, is approximated in terms of EOFs according to

$$\phi(x,t) \approx \sum_{n=1}^{m} a_n(t) v_n(x), \qquad m < N$$

with $a_n(t)$ the amplitude time series and $v_n(x)$ the eigenvectors of the product-moment matrix

$$C(x,y) = \langle \phi(x,t)\phi(y,t) \rangle.$$

Usually an EOF analysis is performed on the anomalies, $\phi(x,t) - \bar{\phi}(x)$, of a particular variable. The EOFs are then the eigenvectors of the corresponding covariance matrix and the amplitudes a_n are uncorrelated and have zero mean. A more detailed discussion of EOF analysis is found in Lorenz (1959).

The EOF analysis is performed on the daily reduced 500 hPa heights rather than on the monthly 500 hPa height anomalies. The reduced 500 hPa heights are obtained by subtracting the daily areal average, $\bar{\phi}(t)$, from the actual 500 hPa height in each grid point and are therefore almost free of a systematical annual cycle. The amplitudes are no longer uncorrelated and their means generally differ from zero. The first three EOFs obtained in this way, however, have a very easy interpretation: the first mode represents a zonal component, the second mode a meridional component and the third mode an (anti-)cyclonic component, while the cumulative percentage of the total variation explained by these EOFs is almost equal to that with the usual EOF analysis. The total variation is defined here as trace $C(x,y)/N$. It thus refers to the total second moment about the daily averages $\bar{\phi}(t)$.

6.1 The CCC EOFs compared with observations

Figure 14 shows the average annual reduced 500 hPa pattern and the first three EOFs of the 1983–1992 ECMWF analyses of the 500 hPa height interpolated to the CCC grid. The orthonormal EOFs are multiplied with the average amplitudes of the EOFs. The first EOF explains 73.4% of the total variation, the second EOF 8.9% and the third mode 5.0%. The average annual reduced 500 hPa pattern and the first three EOFs of the CCC control run (10 years) are presented in Figure 15. The explained variation is 82.6%, 5.7% and 3.5% for the first, second and third mode respectively. The total variation explained in the CCC control run is thus almost 10% higher for the first mode and somewhat smaller for the second and third mode. The EOFs from the CCC control run and the ECMWF analyses have a very similar structure. However the average second mode circulation in the ECMWF analyses is opposite (weakly north) to that in the CCC control run (south).

To compare the average annual amplitudes of the first three EOFs of the ECMWF analyses with those of the CCC control run and the $2xCO_2$ run with the control run, the EOFs of the ECMWF analyses were used as a basis. This involves computing the amplitudes of the CCC patterns from the ECMWF determined eigenstructure. The average annual amplitudes and the interannual standard deviations of the first three EOFs are presented in Table 13. The average second and third mode amplitudes of the CCC control run differ significantly at the 5%-level from those of the ECMWF analyses according to Student's t-test. Differences in standard deviation do not invalidate the use of this test because the sample sizes are equal (Welch, 1938). For the first EOF only the average amplitude of the $2xCO_2$ run differs significantly from the control run. Table 14 shows the average amplitudes and the interseasonal standard deviations for the October–March period. In this period the average first and second EOF amplitudes of the CCC control run are significantly different from those of the ECMWF analyses. Again only the first mode average amplitude of the perturbed run differs significantly from the control run.

An objective circulation classification system can be created by dividing the daily amplitudes of each EOF into three circulation categories. Using only the first three EOFs, combination of these categories results in a classification system with 27 classes which is known at KNMI as the P27 classification (Kruizinga, 1979). The amplitudes of the first EOF are divided into the circulation categories: strong west, neutral west and light west/east. The second mode amplitudes are divided into: north, neutral and south. The circulation catagories for the amplitudes of the third mode are: anti-cyclonic, neutral and cyclonic. The annual EOFs of the 1983–1992 ECMWF analyses are again used as a basis. The catagory boundaries are chosen in such a way that each catagory of a mode contains one third of the events (days) of the 1983–1992 ECMWF analyses.

Table 15 shows the annual frequency distribution of the circulation catagories of the first three EOFs. By definition the ECMWF analyses are uniformly distributed over the catagories. In the CCC control run the number of days with strong west circulation is about 5% larger and the number of days with light west/east circulation is about 5% smaller compared to the ECMWF analyses. Compared with the control run the number of days with strong west flow in the $2xCO_2$ run increases by about 10% mostly at the expense of the light west/east flow frequency. With respect to the second mode in the CCC control run the north circulation frequency is about 18% too small. This shortage is equally compensated by the frequencies of the neutral and south circulation. This indicates that there is too little blocking which is consistent with the lack of blocking near the surface as mentioned in section 2.2. The t-value for the difference in second mode average amplitude (Table 13) is even significant at the 1%-level. The frequency distribution of the second mode circulation catagories does hardly change as a result of a CO_2 doubling. This is consistent with the almost equal average second mode amplitudes for the $1xCO_2$ and $2xCO_2$ runs in Table 13. The CCC control run generates in the third mode 13% too little anti-cyclonic events. The frequencies of neutral and cyclonic circulation are respectively 8 and 5% too high. The CO_2 doubling does also not affect the frequency distribution of the third mode circulation categories. Student's t-test for the difference in the corresponding

average amplitudes results in a non-significant value of the test statistic (Table 13). In general, modes with large differences in the frequency distribution of the circulation catagories also have large (significant) t-values for the difference in the average modal amplitudes.

The frequency distribution of the first three EOF catagories for the period October–March is presented in Table 16. There is in the October–March period a difference of about 15% between the frequencies of the ECMWF analyses and the CCC control run for both strong west and light west/east circulation. The t-value for the corresponding difference in average amplitudes is also significant (Table 14). In the same period the frequencies of the north and south circulation in the CCC control run are respectively 23% smaller and 16% larger compared with the ECMWF analyses. The corresponding difference in the average amplitudes yields again a t-value significant at the 1%-level (Table 14). This under respectively overestimation of the north and south circulation frequencies is in agreement with the wind direction distribution near the surface for the grid points WL and WS (section 2, Figures 4b and 5b). In the third mode circulation categories the differences in frequency distribution are almost the same as for the whole year. The sign of the frequency change due to a CO_2 doubling in the period October–March is for nearly all circulation categories the same as for the whole year. The largest change in frequency is again for the catagory strong west. The corresponding t-value for the difference in average amplitude of the first EOF is the only significant one (Table 14).

Matyasovszky et al. (1993) used 9 circulation pattern (CP) types based on principal components of 500 hPa heights coupled with k means clustering. For the CCC model they found over the U.S. (25°–60°N, 80°–125°W) in general relatively small differences between the CP frequencies of the $1xCO_2$ and $2xCO_2$ simulations as compared to the differences between the frequencies of the $1xCO_2$ simulation and historical data.

6.2 The ECHAM EOFs compared with observations

Figures 16 and 17 show respectively the average annual reduced 500 hPa pattern and the first three EOFs of the 1983–1992 ECMWF analyses interpolated to the ECHAM grid and of the ECHAM control simulation. The first three EOFs of the ECMWF analyses explain 75.7%, 7.6% and 4.7% of the total variation respectively. For the ECHAM control run these numbers are 77.2%, 5.5% and 4.0%. The gradients of the average 500 hPa circulation and of the first EOF are smaller in the ECHAM model and there is a trough over central Europe. The weak circulation was also reported by Roeckner et al. (1992) who studied different versions of the ECHAM model with prescribed sea surface temperatures. In the newer versions (ECHAM 2 and 3) they found an improved circulation over the North Atlantic. The trough in the circulation seems to originate from a westward displacement of the Russian trough due to a shorter Rossby wavelength in the weaker flow. The east side of the trough is a preferential place for the formation of depressions. Indeed, at the same position, the time filtered 500 hPa variability in the storm track (section 5, Figure 13) increases.

The second mode contains an east component for the ECMWF analyses but a west component for the ECHAM control run. The average contribution of the third mode

is in the ECMWF analyses cyclonic but in the ECHAM control run anti-cyclonic. Note, however, that this is a minor effect compared with the strong cyclonality of the first EOF.

The EOFs of the ECMWF analyses interpolated to the ECHAM grid are used as a basis to compare the average amplitudes of the ECMWF analyses with those of the ECHAM model and both perturbed runs with the control run. The average annual amplitudes are presented in Table 17. All three average amplitudes of the ECHAM control run differ significantly at the 5%-level from those of the ECMWF analyses. There are no significant differences between the perturbed runs and the control run. Table 18 shows the average amplitudes for the October–March period. In this period there is a significant difference between the ECHAM control run and the ECMWF analyses for the average amplitudes of the first and third mode. As before no significant differences between the perturbed runs and the control run are found.

Each amplitude is as before divided into three circulation categories. Table 19 shows the annual frequency distributions of the circulation categories in which the ECMWF analyses are again by definition uniformly distributed. In the ECHAM control run the frequency of strong west circulation is about 25% smaller and the frequency of light west/east is about 30% larger compared to the ECMWF analyses. Like the smaller gradient compared with observations this indicates that the 500 hPa circulation in the ECHAM model is on average too weak. The frequency of the south circulation in the ECHAM control run is underestimated by about 15% which is compensated by an equal overestimation of the frequency of the second mode neutral circulation. The frequency of the anti-cyclonic circulation is in the ECHAM control run about 20% too small and the frequencies of neutral and cyclonic circulation are both about 10% too high. The overestimation of the cyclonic circulation can be attributed to the trough in the average 500 hPa pattern which induces an average cyclonic amplitude. The frequency distributions for the perturbed runs are almost equal to those for the control run.

Hulme et al. (1993) obtained similar results over the British Isles (45°–65°N; 20°W–10°E) based on an objective classification of Lamb weather types for the same ECHAM control run. In particular they found an underestimation of the annual frequencies of the (basic) weather types: west, south and anti-cyclonic; and an overestimation of the types: east, north and cyclonic.

The frequency distributions for the October–March period are given in Table 20. In this period the frequency of strong west circulation is about 35% too small in the ECHAM control run. The frequency of the south circulation is again about 15% too small. The anti-cyclonic circulation frequency is about 35% too small and the cyclonic circulation frequency is about 30% too high. The frequency distributions again do not change due to increased CO_2 concentrations.

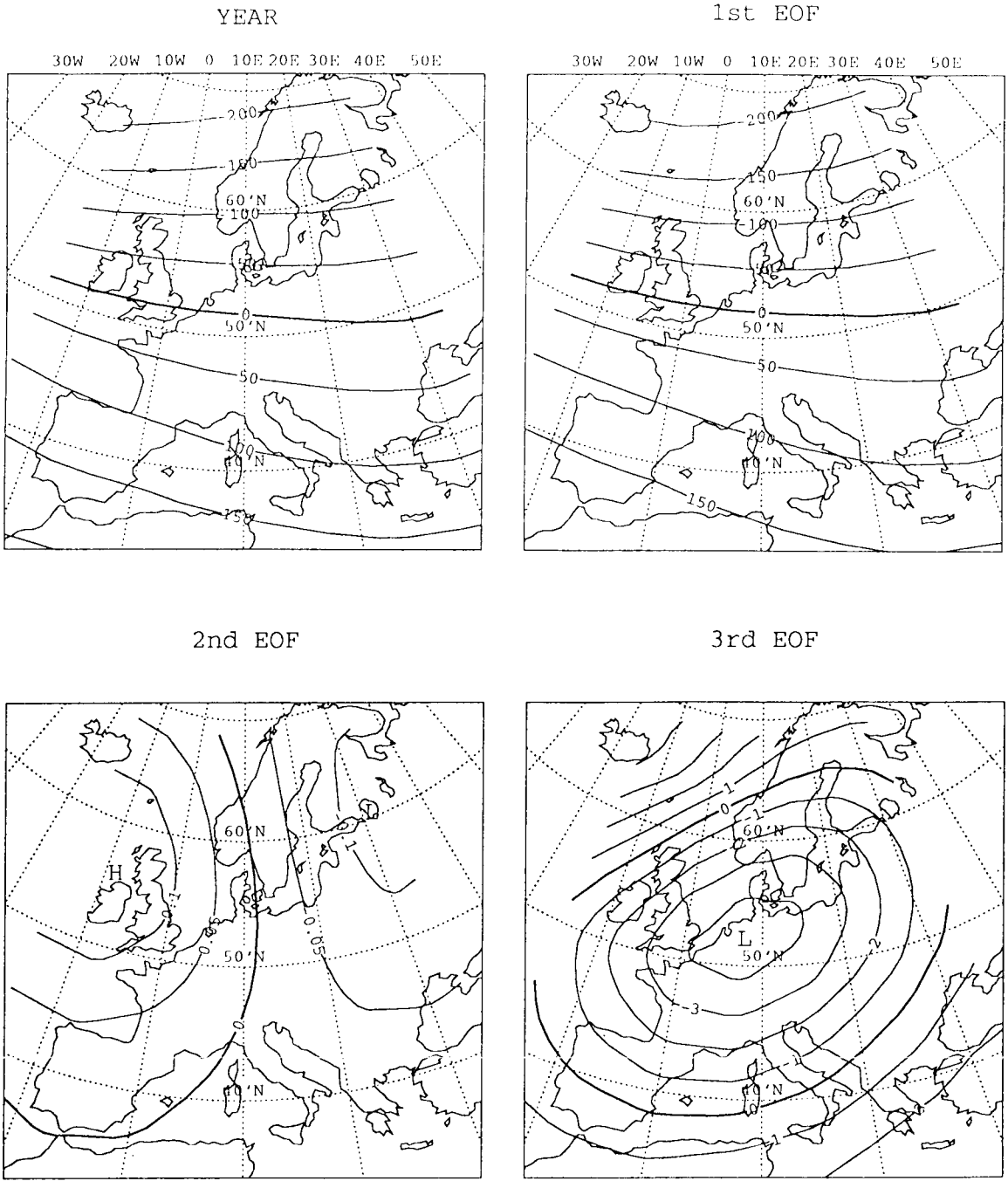

Figure 14: Average annual reduced 500 hPa pattern (upper left panel) and the first three EOFs (upper right, lower left and lower right panels respectively) of the 1983-1992 ECMWF analyses of the 500 hPa height interpolated to the CCC grid. The EOFs explain 73.4%, 8.9% and 5.0% of the total variation.

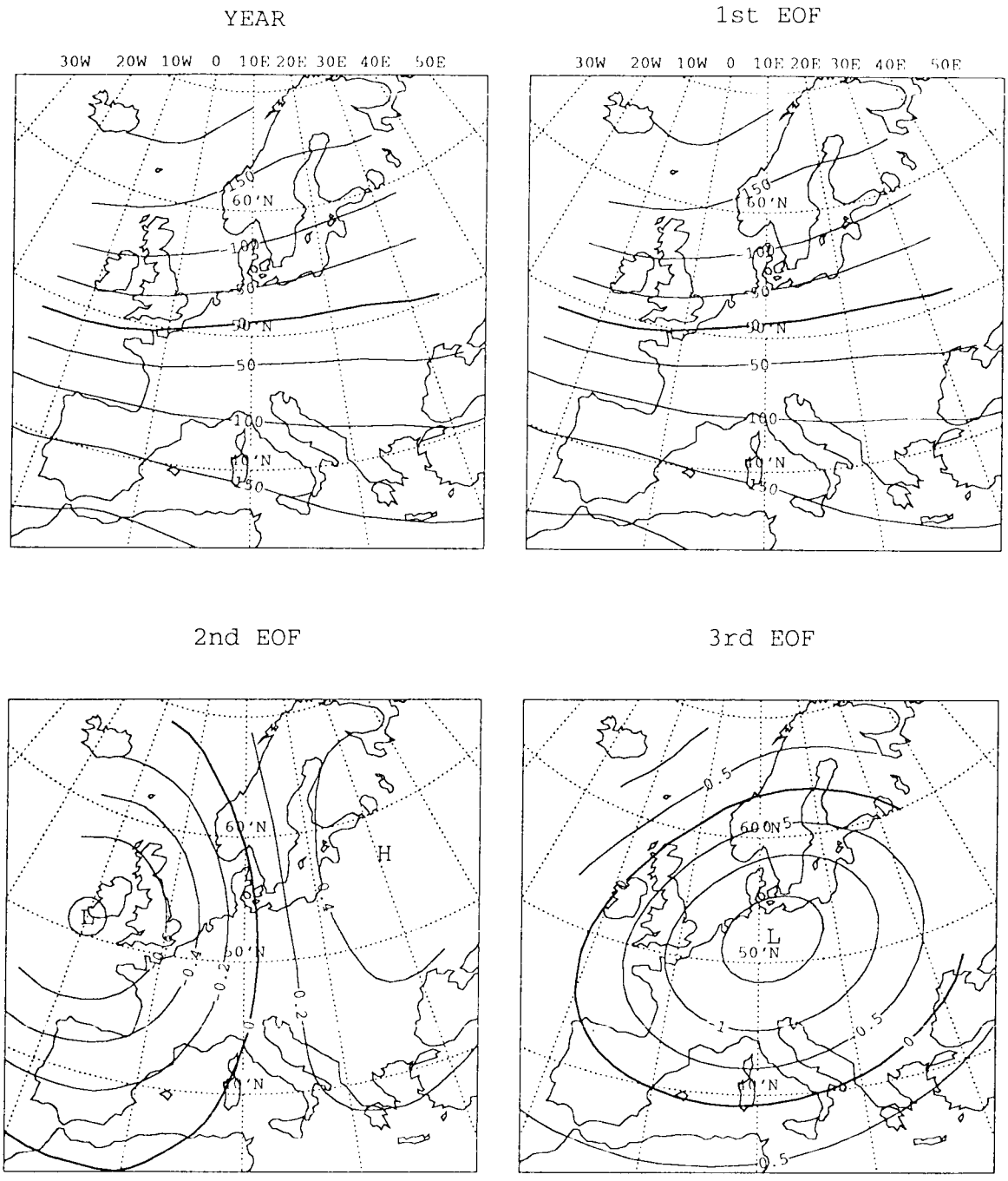

Figure 15: Average annual reduced 500 hPa pattern (upper left panel) and the first three EOFs (upper right, lower left and lower right panels respectively) of the CCC control simulation. The EOFs explain 82.6%, 5.7% and 3.5% of the total variation.

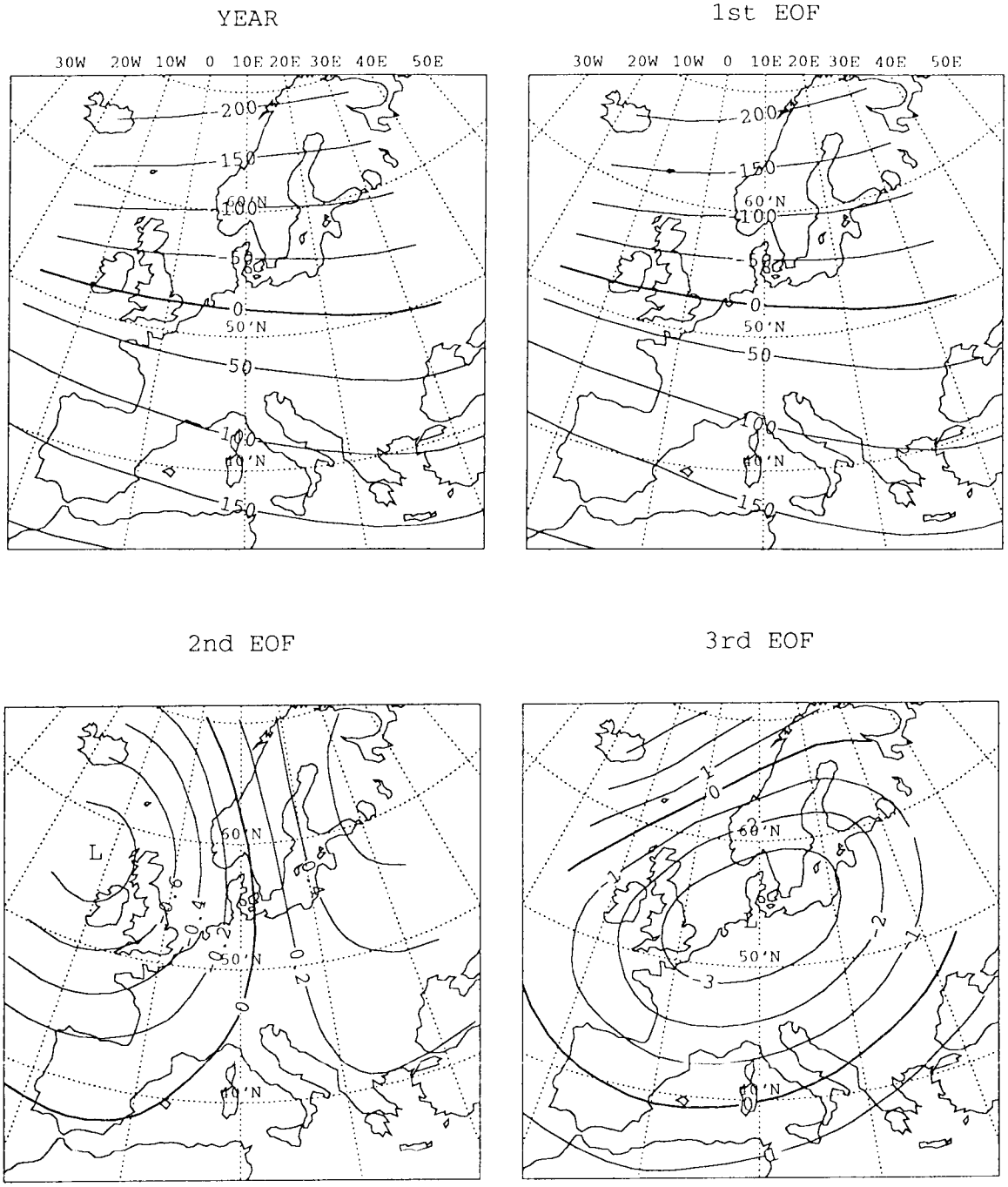

Figure 16: Average annual reduced 500 hPa pattern (upper left panel) and the first three EOFs (upper right, lower left and lower right panels respectively) of the 1983–1992 ECMWF analyses of the 500 hPa height interpolated to the ECHAM grid. The EOFs explain 75.7%, 7.6% and 4.7% of the total variation.

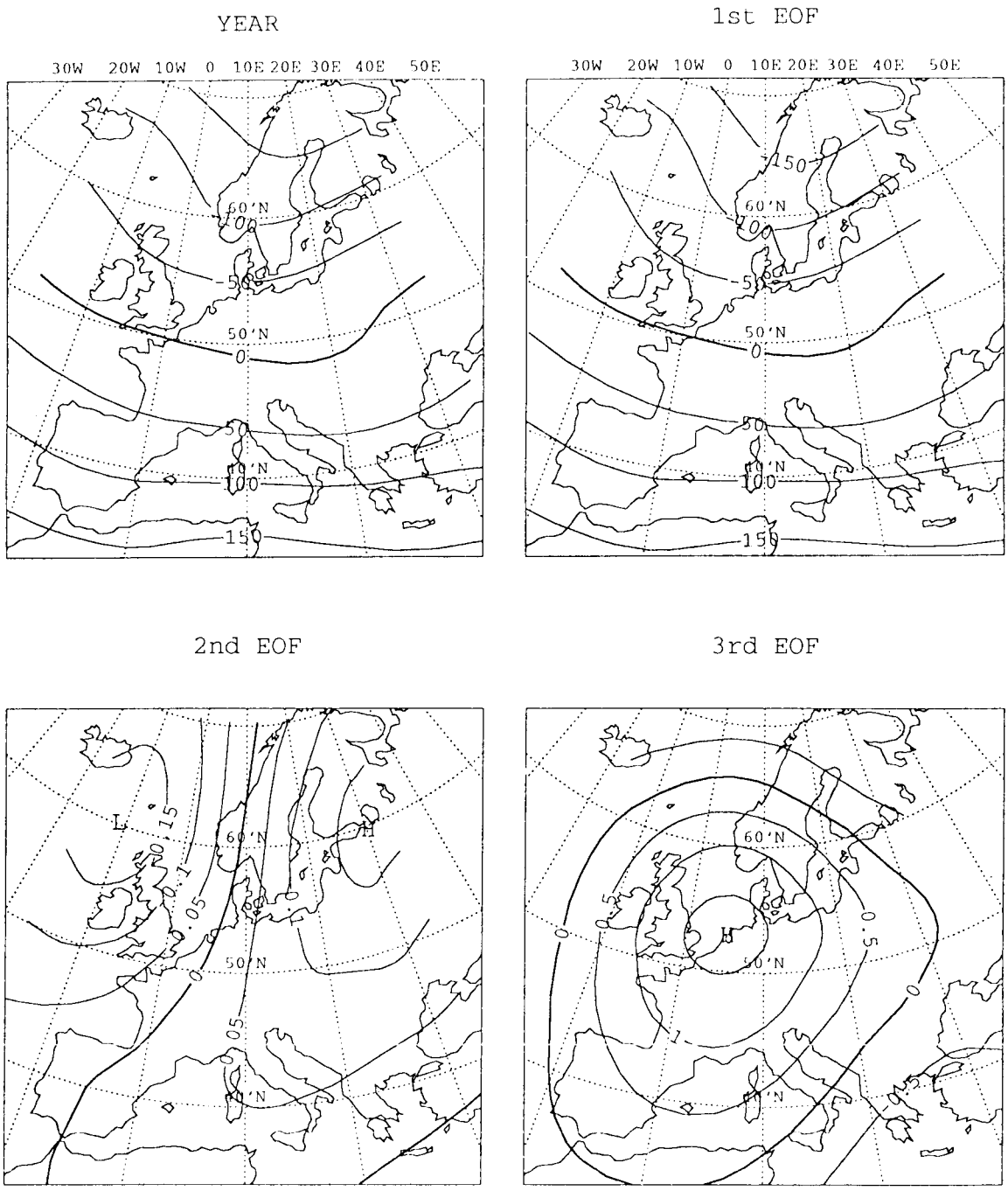

Figure 17: Average annual reduced 500 hPa pattern (upper left panel) and the first three EOFs (upper right, lower left and lower right panels respectively) of the ECHAM control simulation. The EOFs explain 77.2%, 5.5% and 4.0% of the total variation.

Table 13: Average annual amplitudes A_i and interannual standard deviation $\sigma(A_i)$ of the i-th EOF ($i = 1,2,3$) for the reduced 500 hPa patterns of the ECMWF analyses and the CCC simulations, t: Student's t-statistic. The EOFs are based on the ECMWF analyses interpolated to the CCC grid.

	ECMWF 1983-1992		CCC 1xCO$_2$		CCC 2xCO$_2$
A_1	-1642.1		-1731.5		-1880.2
$\sigma(A_1)$	104.3		125.0		73.5
t		-1.73		-3.21*	
A_2	0.8		-196.1		-203.0
$\sigma(A_2)$	70.6		66.9		63.0
t		-6.40*		-0.23	
A_3	-26.1		-115.7		-139.3
$\sigma(A_3)$	91.7		53.6		57.6
t		-2.67*		-0.95	

* t-value significant at the 5%–level

Table 14: Average October–March amplitudes A_i and interseasonal standard deviation $\sigma(A_i)$ of the i-th EOF ($i = 1,2,3$) for the reduced 500 hPa patterns of the ECMWF analyses and the CCC simulations, t: Student's t-statistic. The EOFs are based on the ECMWF analyses interpolated to the CCC grid.

	ECMWF 1983-1992		CCC 1xCO$_2$		CCC 2xCO$_2$
A_1	-1835.8		-2032.9		-2252.9
$\sigma(A_1)$	205.8		167.7		103.8
t		-2.34*		-3.53*	
A_2	120.7		-218.6		-287.7
$\sigma(A_2)$	173.0		116.9		81.1
t		-5.14*		-1.53	
A_3	17.2		-79.7		-141.0
$\sigma(A_3)$	122.4		86.5		91.4
t		-2.04		-1.51	

* t-value significant at the 5%–level

Table 15: Annual frequencies (%) of the circulation categories for the reduced 500 hPa pattern of the ECMWF analyses and the CCC simulations.

	ECMWF 1983-1992	CCC 1xCO$_2$	CCC 2xCO$_2$
1st EOF			
strong west	33.3	38.2	48.8
neutral west	33.3	33.8	29.4
light west/east	33.4	28.0	21.8
2nd EOF			
north	33.3	15.1	14.2
neutral	33.3	43.4	46.1
south	33.4	41.5	39.7
3rd EOF			
anti-cyclonic	33.3	20.4	19.3
neutral	33.4	40.9	40.6
cyclonic	33.4	38.7	40.1

Table 16: October–March frequencies (%) of the circulation categories for the reduced 500 hPa pattern of the ECMWF analyses and the CCC simulations.

	ECMWF 1983-1992	CCC 1xCO$_2$	CCC 2xCO$_2$
1st EOF			
strong west	49.0	61.3	79.0
neutral west	24.3	26.1	18.0
light west/east	26.7	9.6	3.0
2nd EOF			
north	42.1	19.5	13.5
neutral	27.8	31.7	36.5
south	30.1	45.9	50.0
3rd EOF			
anti-cyclonic	39.9	27.0	22.3
neutral	26.7	35.5	35.5
cyclonic	33.3	37.6	42.1

Table 17: Average annual amplitudes A_i and interannual standard deviation $\sigma(A_i)$ of the i-th EOF ($i = 1,2,3$) for the reduced 500 hPa patterns of the ECMWF analyses and the ECHAM simulations, t: Student's t-statistic. The EOFs are based on the ECMWF analyses interpolated to the ECHAM grid.

	ECMWF		ECHAM				
	1983-1992		1xCO$_2$		2xCO$_2$		Scen_A
A_1	-1304.7		-1009.7		-1014.0		-1040.6
$\sigma(A_1)$	80.3		46.4		41.2		38.1
t		10.06*		-0.20		-1.63	
A_2	-3.4		60.5		19.8		26.3
$\sigma(A_2)$	53.1		17.5		60.3		51.9
t		3.61*		-2.05		-1.97	
A_3	-16.4		-159.8		-138.6		-154.8
$\sigma(A_3)$	70.0		34.3		39.8		46.9
t		-5.82*		1.28		0.27	

* t-value significant at the 5%-level

Table 18: Average October–March amplitudes A_i and interseasonal standard deviation $\sigma(A_i)$ of the i-th EOF ($i = 1,2,3$) for the reduced 500 hPa patterns of the ECMWF analyses and the ECHAM simulations, t: Student's t-statistic. The EOFs are based on the ECMWF analyses interpolated to the ECHAM grid.

	ECMWF		ECHAM				
	1983-1992		1xCO$_2$		2xCO$_2$		Scen_A
A_1	-1464.9		-1146.5		-1144.9		-1155.9
$\sigma(A_1)$	156.1		46.2		49.5		60.0
t		6.18*		0.07		-0.39	
A_2	79.0		94.9		69.1		46.8
$\sigma(A_2)$	127.5		32.4		78.9		85.2
t		0.38		-0.96		-1.67	
A_3	11.3		-280.0		-256.5		-254.8
$\sigma(A_3)$	88.3		57.4		45.4		60.6
t		-8.75*		1.02		0.95	

* t-value significant at the 5%-level

Table 19: Annual frequencies (%) of the circulation categories for the reduced 500 hPa pattern of the ECMWF analyses and the ECHAM simulations.

	ECMWF	ECHAM		
	1983-1992	$1xCO_2$	$2xCO_2$	Scen_A
1st EOF				
strong west	33.4	8.7	8.6	9.1
neutral west	33.2	29.9	29.6	33.0
light west/east	33.4	61.4	61.8	57.9
2nd EOF				
north	33.3	33.6	28.7	28.9
neutral	33.3	50.6	51.2	52.7
south	33.4	15.8	20.1	18.4
3rd EOF				
anti-cyclonic	33.4	12.5	12.5	12.1
neutral	33.3	45.5	47.8	44.9
cyclonic	33.4	42.1	39.7	43.0

Table 20: October–March frequencies (%) of the circulation categories for the reduced 500 hPa pattern of the ECMWF analyses and the ECHAM simulations.

	ECMWF	ECHAM		
	1983-1992	$1xCO_2$	$2xCO_2$	Scen_A
1st EOF				
strong west	50.8	15.7	16.2	15.7
neutral west	24.3	40.4	40.4	43.7
light west/east	24.9	43.9	43.4	40.6
2nd EOF				
north	42.4	40.2	38.9	34.9
neutral	27.5	43.1	41.0	43.6
south	30.1	16.7	20.1	21.5
3rd EOF				
anti-cyclonic	40.2	5.5	4.3	6.1
neutral	25.9	31.4	31.9	32.2
cyclonic	33.9	63.1	60.8	61.7

7 Discussion and conclusions

Apart from its mathematical definition it is not clear if a value at a grid point represents the value at that location, the average of the grid box or something complex. It is therefore sometimes argued that time series of individual grid points are not comparable with those of observational stations and that the skill of models just starts at the scale of several grid points (von Storch et al., 1993). Many surface parameters are very sensitive to local conditions. The maximum temperature, for example, depends strongly on the soil type and the soil wetness. Due to the coarse resolution climate models do not resolve small scale phenomena but they are taken into account indirectly by way of parametrisation which causes some sort of average character of grid point values. The surface wind typically depends on stability, pressure gradient (large scale) and terrain roughness (small scale). In general the pressure gradient over a grid box is small and the area being studied has a flat topography. As a consequence, differences in wind from different locations within a grid box mainly result from inhomogeneous land sea transitions in a coastal area (as illustrated in Figure 8). By comparing a land grid point with at least two stations over land the effect of the land sea inhomogeneities is attributed qualitatively and to some extent quantitatively. An alternative would be to compare averages of stations with grid boxes. But then questions arise like how many stations should one use and what should one do if a large part of a land grid box lies over sea? Although it is useful to compare the surface wind at grid points with the observed wind at measurement site it is strongly recommended to investigate how far possible differences can be explained by systematic deviations in the upper air flow.

The CCC model reproduces the average wind speed fairly well over the Netherlands. Although the 500 hPa flow is weak the average wind speed and the frequency of gales are realistic over land in the ECHAM model. In general the differences between the surface wind in the control runs and the observed wind are large compared with the simulated changes due to a CO_2 increase. In particular the almost uniform wind direction distribution in the ECHAM model and the large annual cycle of the wind speed over sea in the CCC model differ very much from those observed. In the latter model the wind speed over sea is in summer even smaller than over adjacent land. The average wind speed and the frequency of gales over the North Sea are reproduced rather poorly in both models.

Study of the storm track reveals an underestimation of the variability of the 500 hPa height in both models. In the ECHAM model the storm track is shifted to the south. Again the differences between the control runs and the observations are larger than the effects of a CO_2 increase.

The meridional component (second EOF) of the 500 hPa circulation in the CCC model differs very significantly from that observed. The average meridional component is south where it should be weakly north. For the surface wind the same situation appears, the land and sea points considered have too little wind from northern directions and too much wind from southern directions. In the CCC model the zonal component (first EOF) of the 500 hPa circulation increases significantly as a result of CO_2 doubling but, except for grid point WS, there are no significant increases in the

gale frequencies.

The average zonal component of the 500 hPa circulation in the ECHAM model is significantly too weak and the flow contains a trough over central Europe. As a result, the average amplitude of the third EOF in the ECHAM model is significantly too cyclonic. There are no significant changes in the amplitudes of the three principal EOFs of the 500 hPa circulation in the ECHAM model as a result of enhanced CO_2 concentrations.

In Summary. From the two models studied it is not clear if there will be any change in the storm activity over the North Sea and the Netherlands due to enhanced greenhouse gas concentrations. The effects of CO_2 doubling are in general very small. The models have difficulties with basic features of the large scale circulation which affect the surface wind. This is clearly demonstrated in the wind direction of the CCC model. In the ECHAM model the weak circulation with the trough over central Europe is probably responsible for much of the discrepancies.

Acknowledgements

The Canadian Climate Centre made their GCM output kindly available. Hans von Storch (Max-Planck-Institut für Meteorologie) arranged the dissemination of the ECHAM simulations and the paper benefited from his critical comments. It is a pleasure to thank Adri Buishand and G.P. Können for many fruitful discussions and suggestions, and C.J.E. Schuurmans for reviewing the manuscript.

References

Blackmon, M.L., 1976: A climatological spectral study of the 500 mb geopotential height of the Northern Hemisphere. *J. Atmos. Sci.*, **33**, 1607–1623.

Boer, G.J., N.A. McFarlane, and M. Lazare, 1992: Greenhouse gas-induced climate change simulated with the CCC second-generation general circulation model. *J. Climate*, **5**, 1045–1077.

Cox, D.R. and D.V. Hinkley, 1974: *Theoretical Statistics*, Chapman and Hall, London.

Cubasch, U., K. Hasselmann, H. Höck, E. Maier-Reimer, U. Mikolajewicz, B.D. Santer and R. Sausen, 1992: Time-dependent greenhouse warming computations with a coupled ocean-atmosphere model. *Climate Dynamics*, **8**, 55–69.

Haarsma, R.J., J.F.B. Mitchell and C.A. Senior, 1993: Tropical disturbances in a GCM. *Climate Dynamics*, **8**, 247–257.

Houghton, J.T., G.J. Jenkins and J.J. Ephraums (Eds.), 1990: *Climate Change. The IPCC Scientific Assessment* Cambridge University Press, Cambridge.

Houghton, J.T., B.A. Callander and S.K. Varney (Eds.), 1992: *Climate Change 1992. The Supplementary Report to the IPCC Scientific Assessment* Cambridge University Press, Cambridge.

Hsing, T., J. Hüsler and M.R. Leadbetter, 1988: On the exceedance point process for a stationary sequence. *Probab. Th. Rel. Fields*, **78**, 97–112.

Hulme, M., K.R. Briffa, P.D. Jones, C.A. Senior, 1993: Validation of GCM control simulaions using indices of daily airflow types over the British Isles. *Climate Dynamics*, **9**, 95–105.

Korevaar, C.G., 1990: *North Sea Climate* based on observations from ships and lightvessels, Kluwer academic publishers, Dordrecht.

Kruizinga, S., 1979: Objective classification of daily 500 mbar patterns. In Preprint Volume: Sixth Conference on Probability and Statistics in Atmospheric Sciences, Banff, Canada, pp 126–129, American Meteorological Society, Boston.

Lambert, S.J., 1988: A cyclone climatology of the Canadian Climate Centre general circulation model. *J. Climate*, **1**, 109–115.

Lau, N.-C., 1988: Variability of the observed midlatitude storm tracks in relation to low-frequency changes in the circulation pattern. *J. Atmos. Sci.*, **45**, 2718–2743.

Lorenz, E.N., 1959: Empirical orthogonal functions and statistical weather prediction. Report No. 1, Statistical Forecasting Project, Dept. Meteorology, MIT

Matyasovszky, I., I. Bogardi, A. Bardossy and L. Duckstein, 1993: Estimation of local precipitation statistics reflecting climate change. *Water Resources Research*, **29**, 3955–3968.

McFarlane, N.A., G.J. Boer, J.-P. Blanchet, and M. Lazare, 1992: The Canadian Climate Centre second-generation general circulation model and its equilibrium climate. *J. Climate*, **5**, 1013–1044.

Roeckner, E., K. Arpe, L. Bengtsson, S. Brinkop, L. Dümenil, M. Esch, E. Kirk, F. Lunkeit, M. Ponater, B. Rockel, R. Sausen, U. Schlese, S. Schubert, M. Windelband, 1992: Simulation of the present-day climate with the ECHAM model: Impact of model physics and resolution. Report No. 93, Max-Planck-Institut für Meteorologie, Hamburg.

Sawyer, J.S.,1970: Observational characteristics of atmospheric fluctuations with a time scale of a month. *Quart. J. Roy. Meteor. Soc.*, **96**, 610–625.

Smith, R.L., 1988: Extreme value theory for dependent sequences via the Stein-Chen method of Poisson approximation. *Stochastic Processes and their Applications*, **30**, 317–327.

von Storch, H., E. Zorita and U. Cubasch, 1993: Downscaling of global climate change estimates to regional scales: An application to Iberian rainfall in wintertime. *J. Climate*, **6**, 1161–1171.

Wallace, J.M., G-H. Lim and M.L. Blackmon, 1988: On the relationship between cyclone tracks, anticyclone tracks and baroclinic waveguides. *J. Atmos. Sci.*, **45**, 439–462.

Welch, B.L., 1938: The significance of the difference between two means when the population variances are unequal. *Biometrika*, **29**, 350–362.

Wieringa, J.,1986: Roughness-dependent geographical interpolation of surface wind speed averages. *Quart. J. R. Met. Soc.*, **112**, 867–889.

van Wijk, A.J.M., A.C.M. Beljaars, A.A.M. Holtslag and W.C. Turkenburg, 1990: Evaluation of stability corrections in wind speed profiles over the North Sea. *J. Wind Eng. Ind. Aerodynam.*, **33**, 551–566.